IOWA STATE UNIVERSITY
Digital Repository

1-1-1983

Neutron detector response to a vibrating absorber located in a fuel assembly

John Thomas Sankoorikal
Iowa State University

Neutron detector response to a vibrating absorber

located in a fuel assembly

by

John Thomas Sankoorikal

A Thesis Submitted to the

Graduate Faculty in Partial Fulfillment of the

Requirements for the Degree of

MASTER OF SCIENCE

Major: Nuclear Engineering

Approved:

Iowa State University
Ames, Iowa
1983

ii

TABLE OF CONTENTS

LIST OF TABLES

LIST OF FIGURES

LIST OF ACRONYMS

UTR-10 - University Training and Research Reactor - 10kW

EW   - East-west

NS   - North-south

APSD   - Auto power spectral density

CPSD   - Cross power spectral density

PRBS   - Pseudo-random binary signal

LVDT   - Linear variable differential transformer

FFT   - Fast Fourier Transform

REG0   - Regulating rod at 0% out

REG100 - Regulating rod at 100% out

UNFLO   - Unflooded

FLO   - Flooded

CIC   - Compensated ion-chamber

HP   - Hewlett Packard

I. INTRODUCTION

The interest in noise analysis stems from its potential use as a surveillance tool. There are numerous driving sources (1,2) of mechanical, thermal, hydraulic and neutronic nature inside a reactor core that cause fluctuation in various process variables of the reactor such as the neutron field, temperature, pressure, etc. These induced fluctuations in neutron population are recorded as neutron noise by in-core and ex-vessel neutron detectors.

The purpose of this study is to investigate some of the basic characteristics of the noise generated by mechanical vibrations of reactor components such as control rods, fuel rods, etc. It is possible (3-14) to locate the vibrating component and measure the magnitude of its vibration by analyzing the noise in neutron detector signals resulting from the vibration. Proper interpretation of these signals would provide a means for early detection of possible mechanical breakdown. Theoretical analysis (6-14) shows that the response of detectors depends on their position relative to the vibrating component. It has been shown that the neutron noise generated can be divided into two components; a space dependent 'local' component and a largely space independent 'global' component. The space dependence of

the local component can be utilized for localization, however, the detector response may be modified because of the interaction between the local and global components. Various techniques are used for noise analysis. In the time domain, auto correlation and cross correlation are used and in the frequency domain, power spectral density and cross power spectral density techniques are used. The cross power spectral density (CPSD) phase between detector signals would also provide information regarding the position of the absorber.

An experiment performed using the UTR-10 reactor at Iowa State University to study the detector response to a vibrating absorber located in a fuel assembly is described in this thesis. Experimental vibration studies performed by Al-Ammar (4) and Borland (5) were restricted to the central vertical stringer, which is in a reflector region. They were able to observe the local and global components of the noise predicted by theory. The noise generated in a fuel region, however, has different characteristics, and furthermore it is more representative of what might be encountered in actual application to a power reactor. Therefore, there is an interest in doing the measurements in the fuel region. A preliminary

investigation for the experiment was done by Salih (8) using the detector adjoint technique.

In this thesis, a theoretical background for the experiment was developed using the Green's function technique to solve the equation for the detector response to a vibrating absorber. An empirical model, based on the local-global concept, was also developed to aid in the interpretation of the experimental data. An experimental apparatus consisting of a vibrating neutron absorber which could be located in a modified fuel assembly was designed and constructed. The design was such that it was possible to have the absorber move in one of two perpendicular planes and measurements could be carried out with the thimble in which the absorber moved unflooded or flooded with water. One drawback of the apparatus was that there was room for only one detector in the core at any time. The experimental data obtained using both single frequency and pseudo-random excitation were analyzed using a Frequency Spectrum Analyzer and a Microcomputer system. The results obtained were compared to theoretical predictions regarding the local-global interaction. Calculations of

the local to global ratio, which is an indicator of
the distance of the vibrating absorber from the detector,
were done only for one mode (east-west) of vibration.
The usefulness, for vibration monitoring, of other data
obtained from the analyzer was also investigated.

II. LITERATURE REVIEW

The importance of neutron noise analysis for the development of vibration monitoring and surveillance systems has been recognized for several years. Measurements on several reactor systems (4-6, 15-19) showed that the spectral behavior of neutron noise signals could be related to the reactor internal vibrations. There have been many theoretical investigations (4, 6, 7-9, 11-14) performed to obtain better understanding of the problem.

The noise induced by the vibrations of a faulty control rod was observed by Stephenson et al. (15). Using a point reactor model, Robinson (16) was able to explain the observed spectrum. Lucia et al. (17) was able to correlate the noise spectra and fuel element vibrations recorded by accelerometers attached to them. The observed double frequency effect was explained by Pazsit (11). The detection of internal vibrations in power reactors is also reported by a number of authors (20-23).

While trying to understand the thermal hydraulics of a boiling water reactor, Van Dam (24) and Behringer et al. (25) showed that the noise generated by moderator density fluctuations can be separated into space dependent 'local' and space independent 'global' components.

Some of the earlier analyses (26, 27) used one-energy group point reactor models to study power reactor noise. In a large power reactor, one would expect the noise to be space dependent. Pazsit (11) used a one-group model to show that the neutron noise field around a vibrating absorber is space dependent. He suggested the use of this space dependence for localization of the vibrating component, but this would require at least two-dimensional models. Later, Pazsit (12) used a semi-analytical, one-dimensional, two-group model to treat a reflected reactor. The analysis was based on the adjoint technique introduced by Van Dam (28), and it was concluded that the local effect in the reflector has a different importance than in the core. In order to deal with more realistic two-dimensional control rod vibrations, Pazsit and Analytis (13) developed a theoretical model using modified one-group theory. The use of the Green's function, which reflects the transfer characteristics of the system, showed that the spatial variation of the noise in two dimensions is more pronounced than for the one-dimensional case. Further, the possibilities of localizing and sizing the vibration were investigated by the above authors. Analytis (14), using a three-dimensional two-group model and the Green's function

technique, showed that the fluctuations in both fast and thermal neutron population can be written as the sum of local and global components. He also showed that the local component has a smaller attenuation length compared to that of the global component. The author also showed the equivalence of the Green's function approach and the dynamic adjoint function formulation (25). Pazsit et al. (7) summarized the theoretical methods of calculating vibration induced neutron noise with application to localization. He points out that a detailed numerical evaluation of the transfer function for each individual plant would be necessary. Lee and Albrecht (9) derived the frequency dependent two-group diffusion equation and used the adjoint technique to solve the problem of two-dimensional control rod vibrations. They discuss a 'contour' (points with equal response for a random vibration at a certain location) method to localize a vibrating control rod.

A report of the work done at Iowa State University can be found in reference (6). Theoretical models (4, 8, 29) were developed for the UTR-10 to obtain the detector response to a vibrating absorber. The two-

dimensional Green's function technique was used by Hennessy (29) to model the reactor response to a moving absorber. Experimental measurements were carried out in the reflector region (4, 5, 29). The results obtained showed the long range global and the short range local components and their interaction. The results obtained were used to estimate the local to global ratios for the detector-vibrator configurations used in the studies.

Danofsky (10) points out that the terms in the detector response should be called, more correctly, the point reactor term and the higher harmonics, corresponding to the global and local terms. This approach is used in this work.

III. THEORETICAL ANALYSIS

A brief discussion of the theoretical basis for the vibrating absorber experiment is given in this section. The Green's function technique is used to derive the response of a neutron detector to the vibrating absorber. The explanation of the results can also be based on an 'empirical' model and is developed in section C.

A. Detector Response to a Vibrating Absorber

The response of a detector, in the frequency domain, to a small fluctuation of the neutron flux, $\delta\phi$, can be written as (4)

$$\delta R(r,\omega) = \int_{V_d} \delta\phi(r,\omega)^T \Sigma_d(r,\omega) dr , \qquad (3.1)$$

where Σ_d is the detector cross section and V_d is the detector volume. Usually, the thermal noise is of interest, therefore, in a two-group development

$$\Sigma_d(r,\omega) = \begin{bmatrix} 0 \\ \Sigma_{d2} \end{bmatrix} . \qquad (3.2)$$

An alternate representation of the detector response using the detector adjoint function (φ^+) is (12, 24, 4, 5) $\int_{V_s} \delta S^T \varphi^+ dr$, where V_s represents all the perturbing sources (δS).

The fluctuation in neutron flux is induced by a

noise source, like the vibration of a control rod. For
the case of the two-dimensional vibrations of an infinitely
thin absorber rod, the noise source can be written as (13)

$$\delta S(r_a, \omega) = \gamma \int_{-\infty}^{\infty} dt \; e^{-i\omega t} \phi(r_a) \left\{ \delta(r_a - r_p - \delta r(t)) - \delta(r_a - r_p) \right\},$$
(3.3)

where γ is the strength of the absorber, r_a (x_a, y_a),
r_p (x_p, y_p) and $\delta r(t)$ $(\delta x(t), \delta y(t))$ are the position,
equilibrium position and the two-dimensional mechanical
trajectory of the absorber rod, respectively, and $\phi(r_a)$
is the static thermal neutron flux.

An expression for $\delta\phi$ can be obtained as follows
(4, 5, 13, 29): The diffusion equation can be written in
matrix form as (4)

$$L(r,t)\phi(r,t) = 0,$$
(3.4)

where L is the diffusion matrix and ϕ is the multigroup
neutron flux vector. It is assumed that the rod vibration
induces small stochastic fluctuation in group parameters.
For example, if the thermal absorption cross section is
perturbed, $\Sigma_a(r,t)$ and $\phi(r,t)$ can be written as

$$\Sigma_a(r,t) = \Sigma_{a0}(r) + \delta\Sigma_a(r,t)$$
(3.5a)

$$\phi(r,t) = \phi_0(r) + \delta\phi(r,t).$$
(3.5b)

Other parameters, like D, Σ_f, etc., are assumed to be constant. Following the procedure detailed in (5), where the perturbed variables are substituted into (3.4) and the equations linearized and transformed to the frequency domain, the equation for the frequency dependent flux is obtained as

$$L(r,\omega)\,\delta\phi(r,\omega) = \delta S(r,\omega), \tag{3.6}$$

where δS describes the frequency dependent noise source composed of the fluctuations of the group parameters multiplied by the static flux. To solve equation (3.6) for $\delta\phi$, the Green's function technique can be used (13, 14, 29, 30).

The Green's function $G(r,r_p,\omega)$ satisfies the equation

$$LG = \delta(r-r_p), \tag{3.7}$$

where r_p is the perturbation point and G satisfies the same boundary conditions as $\delta\phi$ in (3.6). Note that the noise source in (3.7) is a point perturbation. A functional form for G can be obtained as outlined in references (11, 13, 30, 31). The solution to equation (3.6) can now be written in terms of G as

$$\delta\phi(r,\omega) = \int_{V_r} dr_p\ G(r,r_p,\omega)\,\delta S(r_p,\omega), \tag{3.8}$$

where V_r is the volume of the reactor and r is the observation point (position of the detector). Note that G can be thought of as the transfer function between the point of observation and the perturbation(s).

To obtain an expression for the detector response, substitute (3.3) into (3.8) and perform the space integration which, with the help of the δ function, yields

$$\delta\phi(r,\omega) = \gamma\int_{-\infty}^{\infty} dt\ e^{-i\omega t}\left\{G(r,r_p+\delta r(t))\phi(r_p+\delta r(t))-\right.$$
$$\left.G(r,r_p)\phi(r_p)\right\}. \tag{3.9}$$

The Fourier transform of the two-dimensional Taylor series expansion of $G(r,r_p+\delta r(t))\phi(r_p+\delta r(t))$ about r_p with the first order terms retained yields

$$\delta\phi(r,\omega) = \gamma\nabla_{r_p}\left[G(r,r_p)\phi(r_p)\right]\cdot\delta r(\omega), \tag{3.10}$$

where in two dimensions

$$\nabla_{r_p} = i\frac{\partial}{\partial x_p} + j\frac{\partial}{\partial y_p} \tag{3.11a}$$

$$\delta r(\omega) = i\delta x + j\delta y. \tag{3.11b}$$

The detector response is given by equation (3.1). The auto power spectral density (APSD) of the detector response

is given by (32)

$$APSD = \delta R^{*}(r,\omega)\delta R(r,\omega) \qquad (3.11c)$$

where '*' represents the conjugate operation. From (3.10) it is evident that the APSD of the detector response will contain any frequency present in the vibration of the absorber. A better understanding of the terms involved in (3.10) can be obtained by considering a simple model.

B. Application to a Rectangular Slab Reactor

The following analysis shows that the noise generated by a randomly vibrating absorber consists of a point reactor term as well as the higher harmonics (10). One may call the point reactor term the reactivity (global) response and the higher harmonics the space dependent (local) term as explained in previous works (4, 5). The following model is taken from reference (13). Consider an absorber located at r_p vibrating in one dimension in a rectangular slab reactor of sides a and b. For this case, equation (3.10) reduces to

$$\delta\phi(r,\omega) = \gamma\left\{\phi\frac{\partial G}{\partial x_p} + G\frac{\partial \phi}{\partial x_p}\right\}\delta x(\omega). \qquad (3.12)$$

The steady state flux and the Green's function are

given by (13)

$$\phi(x_p, y_p) = \phi_0 \sin(B_{1x}x_p)\sin(B_{1y}y_p) \tag{3.13}$$

$$G(r, r_p, \omega) = \frac{-4}{ab} \sum_{m=n=1}^{\infty} \left(\sin(B_{mx}x)\sin(B_{mx}x_p)\sin(B_{ny}y) \right.$$
$$\left. \sin(B_{ny}y_p) \right) / \left(B_{mx}^2 + B_{ny}^2 - B^2(\omega) \right)$$

$$\tag{3.14}$$

where

$$B_{mx} = \frac{m\pi}{a}, \quad B_{ny} = \frac{n\pi}{b}, \quad B^2(\omega) = B_0^2(1 - \epsilon(\omega)) \quad \text{and}$$

$$\epsilon(\omega) = \frac{K_\infty}{M^2 B_0^2 G_0(\omega)} , \tag{3.15}$$

where $G_0(\omega)$ is the zero power reactivity transfer function, B_0^2 is the geometrical buckling and K_∞ is the infinite multiplication factor of the reactor. The migration area M^2 is introduced to account for fast leakage. The point-reactor term is obtained by setting m=n=1 in the Green's function (13). Substituting (3.13) and (3.14) into (3.12) and keeping the m=n=1 term separate yields,

$$\delta\phi(r, r_p, \omega) = -K\phi_0 B_{1x} \sin(B_{1x}x)\sin(B_{1y}y)2\sin(B_{1x}x_p)$$

$$\cos(B_{1x}x_p)\sin^2(B_{1y}y_p)\delta x(\omega) \ +$$

Higher Harmonics (m=n=2 to ∞ in G)   (3.16)

where K is a constant. From equation (3.16), the
following conclusions can be made regarding the global
or point-reactor response:

1.   If the vibrator is located at the center of the
reactor where the flux gradient is zero, the global
contribution to $\delta\phi$=0 since $B_{1x}x_p = \pi/2$.

2.   If the vibrator is located in a region where the
flux is increasing with x, (0-a/2), and if δx is positive
in the x direction, the global contribution is negative
since the cosine term is positive. On the other hand, if δx is
negative in the x-direction the global contribution is
positive. Thus, if the vibrator is moving up the gradient
the increased negative reactivity reduces the global flux
in the reactor and vice versa.

3.   The global response depends on the detector
position (x,y) which means that for two detectors located
at different positions, different responses will
result even if the absorber position remains the same.

4.   Also note that the response changes with the

vibrator position (x_p, y_p).

These conclusions will be useful in analyzing the data obtained from the experiment.

As an alternate viewpoint, the global and local components are characterized by their different attenuation lengths (14). The global component will be effective over a large volume around the perturbation while the local component drops off faster with distance from the perturbation. The higher harmonics terms in (3.16) represent the local component of the total response. One could consider the local effect as being produced by the movement of the local flux depression of the absorber.

The space dependence of the local effect can be used for localization of the absorber, but this is complicated by the fact that when the absorber is moving in a gradient the global response part could be negative or positive. Since the global effect is largely space-independent, a local to global (L/G) ratio can be defined which would be a measure of the distance of the absorber from the detector. The empirical model given in the next section describes the procedure used to calculate the L/G ratio in the case when the detectors are located along the direction of vibration.

C. Empirical Model

1. Explanation of the local-global interaction

As illustrated in Figure 3.1, consider an absorber
moving in the east-west (EW) direction in the presence of
a positive flux gradient from west to east. Two detectors
(1E and 1W) are located symmetrically on the east and
west side of the absorber. As the absorber moves to the
east, the east detector sees a local flux depression
moving towards it as well as a drop in the entire reactor
flux, which is the global effect. These two effects are
in-phase or in other words they add together for the east
detector. At the same time for the west detector, the local
contribution increases while the global component decreases.
Thus, the two effects are out-of-phase, and they subtract
for the west detector. This addition or subtraction of
local and global components will alter the responses of
detectors to the vibrating absorber and depends on their
location relative to the absorber. It is possible that
these two effects can have the same magnitude, and in this
case, the detector for which the two effects subtract
would see no change at all.

2. Calculation of the local to global ratio

As pointed out in section IV, due to physical
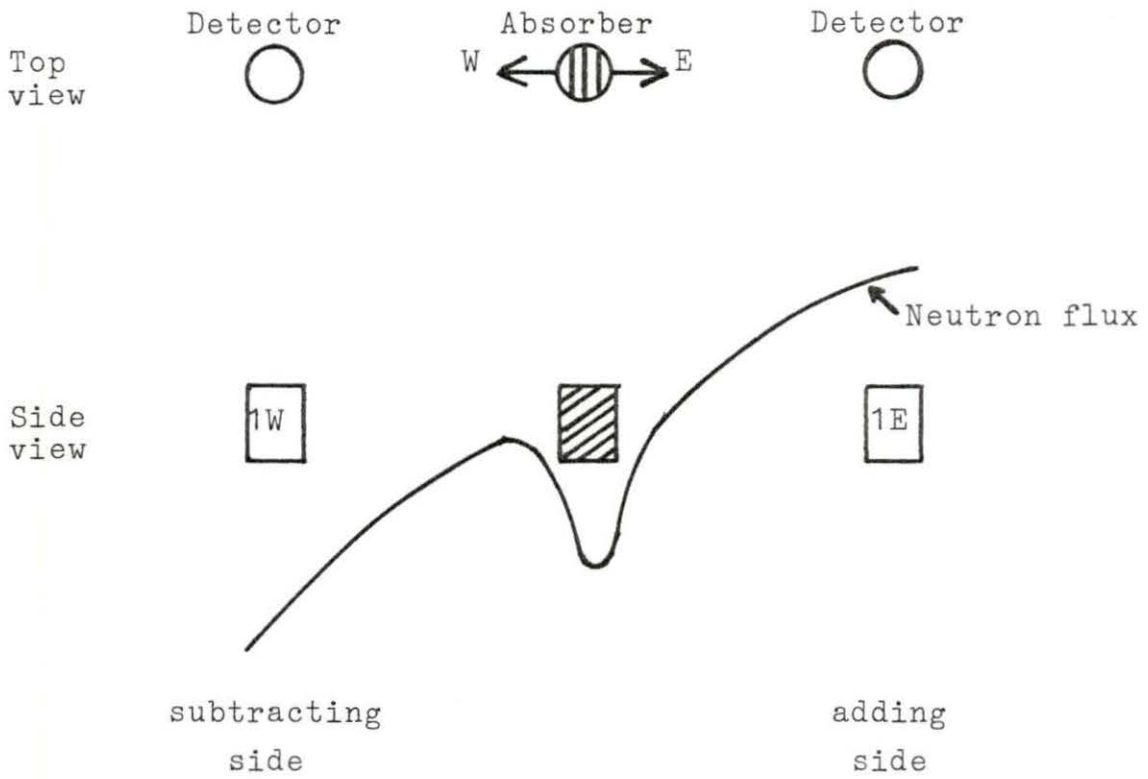
Figure 3.1. Explanation of the local-global interaction

constraints, it was possible to use only one detector (D_1) in the core for the experiment. It was possible, however, to interchange the location of the vibrator and the detector to simulate the case of the detectors on the east and west (D_{1E}, D_{1W}) side of the absorber. The global components seen by the detector on either side will be different since the reactivity change will be different for each position and the detector position has also been changed. The global component when the detector is on the west side is designated as G_{1W} and that for the east side as G_{1E}. The local components (L) were assumed to be the same since the absorber-detector separation was unchanged. A second detector (D_2) was placed in the thermal column. It can be assumed that this detector sees only the global effect and that it is a constant fraction of the global effect observed by the detector D_1. Thus, when D_1 is on the west, the response of D_2, G_{2W}, is given by CG_{1W}, where C is a constant. Similarly G_{2E} is given by CG_{1E}. The constant C is assumed to be the same for the two cases.

If the linear variable differential transformer (LVDT) signal is taken as the reference, the global effect (G_{1E}, G_{1W}, G_{2E}, G_{2W}), a reactivity effect, lags the LVDT signal by the angle determined by the reactor reactor transfer function, as shown in Figure 5.6. The local

component was assumed to be real. The local component observed by the east detector, L_E, is in phase with the LVDT signal while that observed by the west detector, L_W, is out of phase with the LVDT signal. The detector responses X_{1E} and X_{1W} are equal to the vector sums of L_E, G_{1E} and L_W, G_{1W}. If the transfer function phases between the LVDT and X_{1W}, θ_W and the LVDT and X_{1E}, θ_E are known, the law of cosines yields

$$G_{1E}^2 = X_{1E}^2 + L^2 - 2X_{1E}L\cos(180-\theta_E) \qquad (3.17)$$

$$G_{1W}^2 = X_{1W}^2 + L^2 - 2X_{1W}L\cos(\theta_W). \qquad (3.18)$$

where it is assumed that $L_W = L_E = L$.
Also,

$$G_{2E} = CG_{1E}, \qquad (3.19)$$

and

$$G_{2W} = CG_{1W}. \qquad (3.20)$$

A quadratic equation in L is obtained by substituting (3.19) and (3.20) in (3.17) and (3.18). The two solutions for L can be substituted into equations (3.17) and (3.18) to get two possible values for G_{1E} and G_{1W}. The ratio

L/G_{1E} and L/G_{1W} for each value of L is then obtained.
The choice between the two possible values for the L/G
ratio, at the two locations east and west, can be made
based on the following criteria:

a. The L/G ratio cannot be negative.

b. The L_W/G_{1W} ratio must be greater than one, if the
phase between D_{1W} (note that this is opposite to X_{1W}) and
the LVDT is close to zero which means that L_W is greater
than G_{1W}.

c. When L and G are of the same magnitude, which is a
conclusion that can be drawn from the phase measurements,
L_E/G_{1E} must be near to one.

Another case looked at was that of the detectors
placed perpendicular to the direction of vibration. Only
qualitative results could be obtained from the measurements
and an empirical model for this particular case was not
developed. These results are discussed in section V.

The phase of the cross power spectral density (CPSD)
between two detectors (for example θ_W - θ_E in Figure 5.6)
may also provide information that can be used for localiza
localization. If the detectors are on either side of
the vibrating absorber along the direction of vibration,
because of the addition and subtraction effects
of the local and global components, the two signals

will be out of phase if the detectors are in the range to
see the local effect. On the other hand, if the detectors
are located symmetrically on a line perpendicular to the
direction of vibration, both the detectors have the same
response, the signals are in phase, and the CPSD phase
is zero. This suggests that a zero CPSD phase does not
always imply that there are no vibrations, as the vibrations
can be perpendicular to the line between the detectors.

IV. EXPERIMENTAL APPARATUS AND PROCEDURES

A. Experimental Apparatus

1. The UTR-10 reactor

The UTR-10 nuclear reactor (33) is a 10kW,
heterogeneous, light water moderated and cooled, graphite
reflected system. Two aluminum core tanks (51cm x 16cm x
145cm deep), separated by a distance of 46cm, are embedded
in a graphite stack 142cm long, 112cm wide and 122cm deep.
Each core tank holds six fuel assemblies and each assembly
is made up of twelve full, half, quarter or zero load fuel
plates. The full load plate contains approximately 22gm
of U-235. The fuel plates are 7.6cm wide, 66cm long and
0.2cm thick including the aluminum cladding of thickness
0.05cm on either side. The fuel is an aluminum-uranium
alloy, with uranium enriched to about 93% in U-235.
The separation between the fuel plates is about 1cm. The
four control rods, two safety type, one shim safety and
one regulating rod, are located in the reflector adjacent
to the core tank. The regulating (and shim safety) rod
can be positioned anywhere between 0% and 100% of
the fully withdrawn position. Figures 4.1 and
4.2 show the plan and elevation of the reactor, and
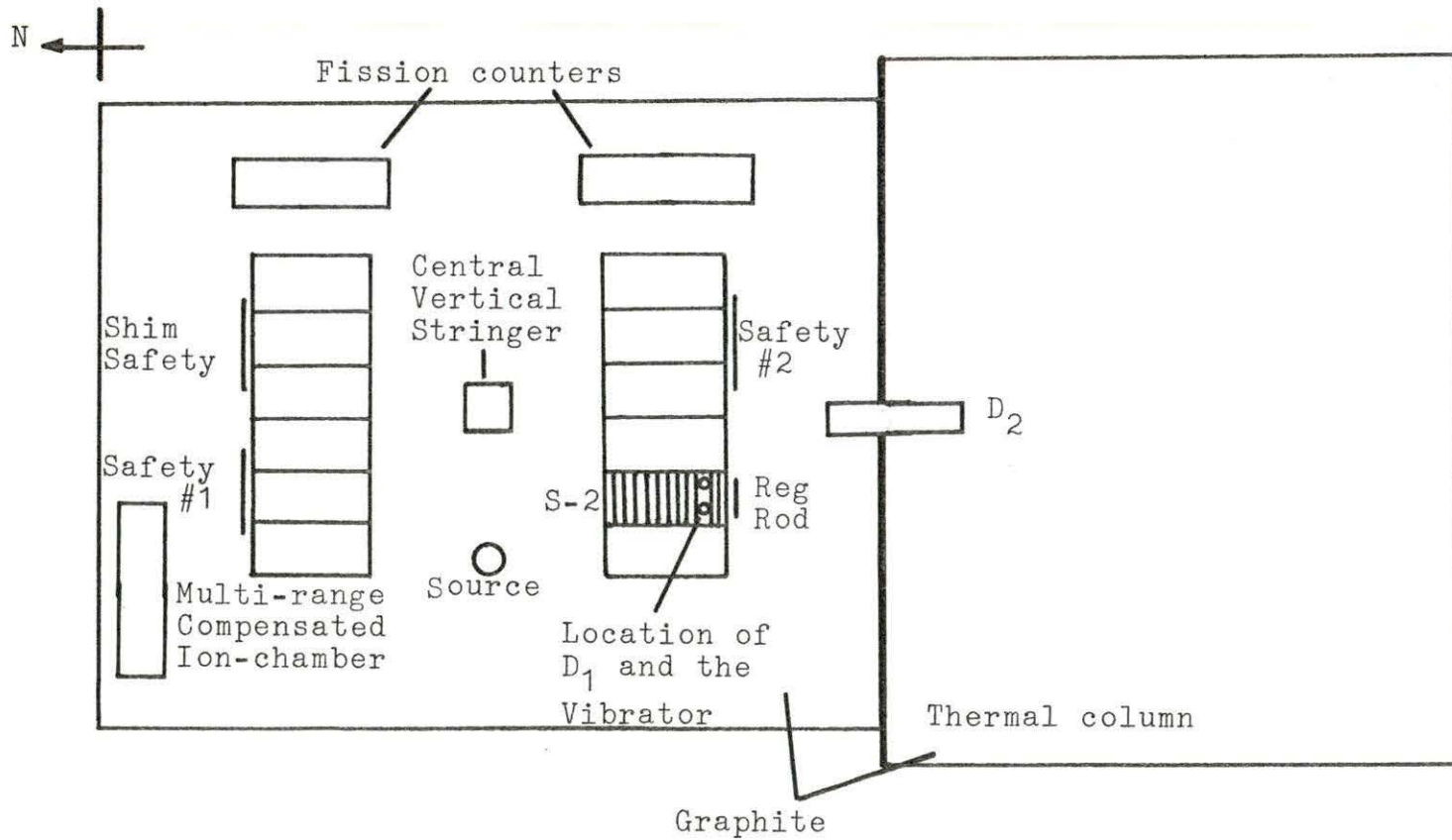
Figure 4.1.   Plan view of the UTR-10 reactor
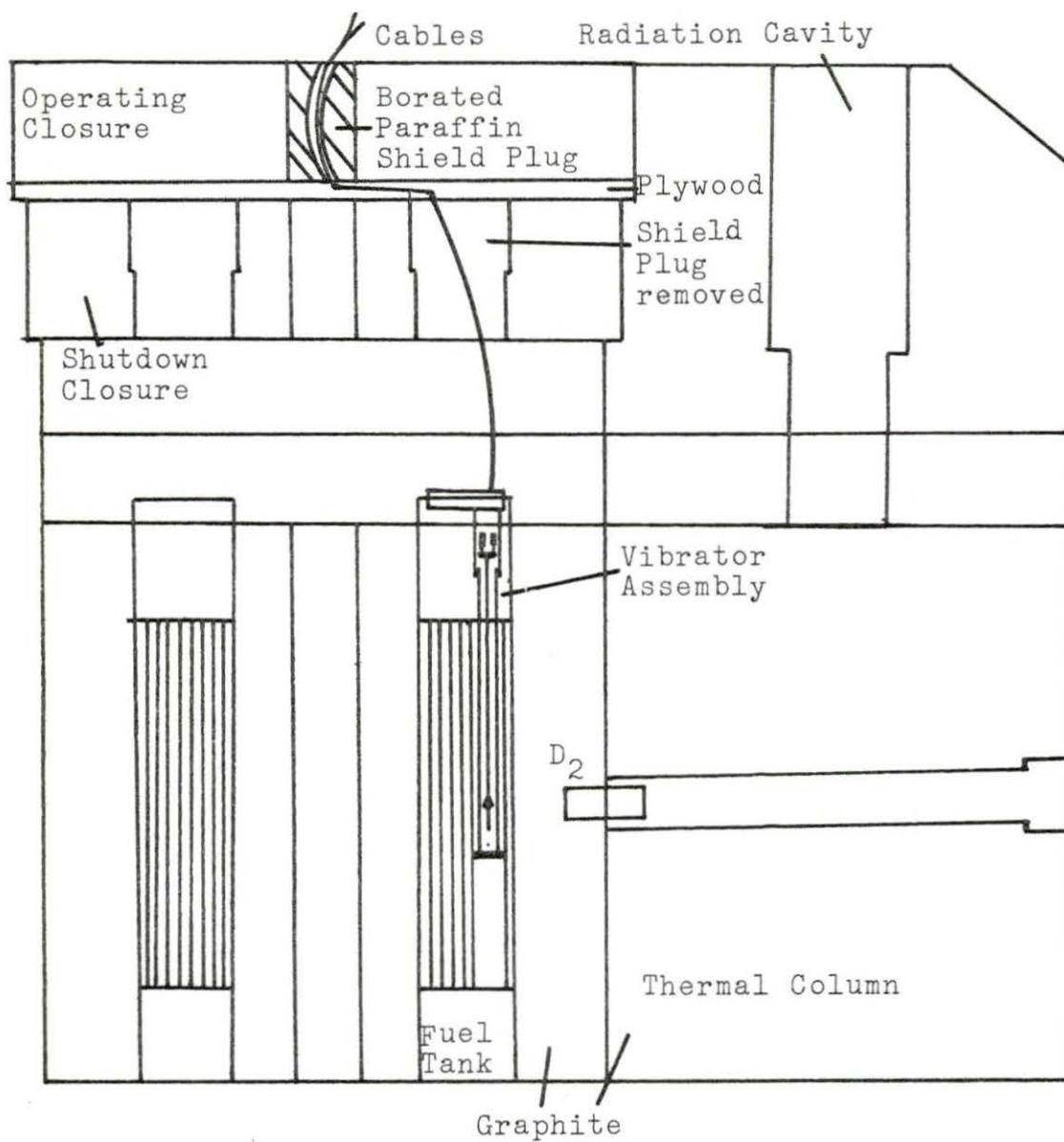
Figure 4.2. Elevation of the UTR-10 reactor

Figure 4.3 shows the drawing of the modified fuel assembly.

The location of the experiment was in S-2 (Figure 4.1) with the vibrator and the in-core detector (D_1) located towards the south side in a gap of about 2.2cm, obtained by removing the third fuel plate from the south side of the assembly. The original fuel loading pattern with the modified fuel assembly did not provide enough excess reactivity for the experiment. To obtain the required excess reactivity, the fuel elements were shuffled and the final loading pattern (B-1), as shown in Figure 4.4, was used for the experiment.

2. The vibrating absorber apparatus

The details of the apparatus are shown in Figures 4.5a and 4.5b. It consists of a 9cm x 0.85cm x 0.05cm cadmium strip attached to an aluminum rod pivoted at the top. Two push type DC coils are placed such that when power is applied to them alternately, they move the rod back and forth resulting in the vibrating motion of the absorber with a maximum peak-to-peak amplitude of about 1.25cm. The linear variable differential transformer (LVDT) attached to the rod measures the position of the absorber.

The entire apparatus sits inside an aluminum thimble
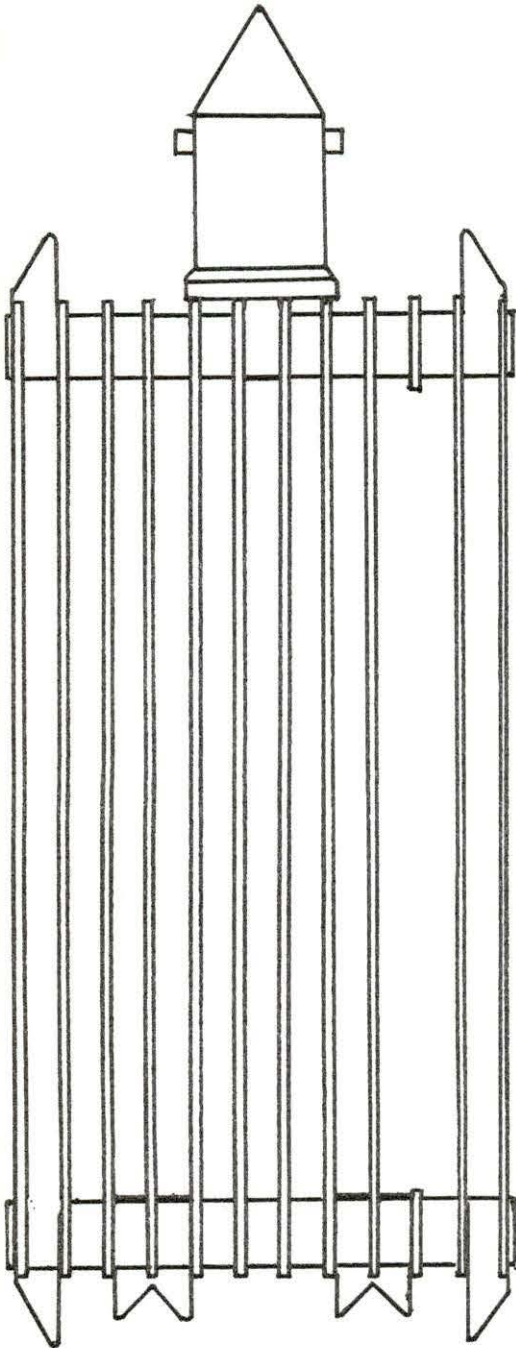
Third Fuel Plate removed
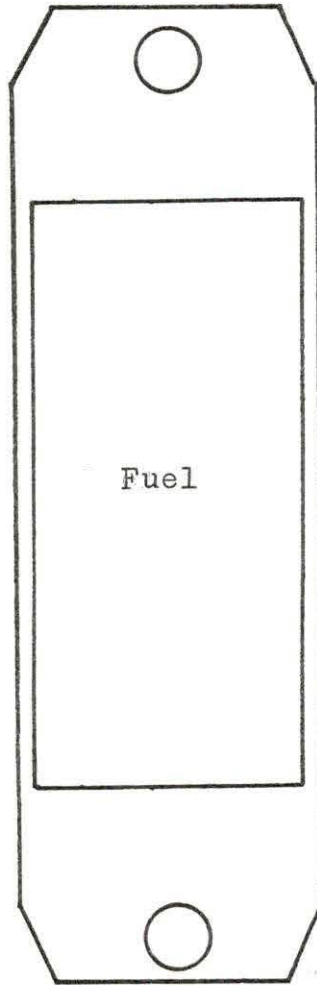
Fuel Plate

Figure 4.3. Fuel assembly after modification

N-1	N-2	N-3	N-4	N-5	N-6
240*	262	262	262	262	196

S-1	S-2	S-3	S-4	S-5	S-6
229	240	262	262	262	240

Location of
Experiment

* Grams of U-235

Figure 4.4. Fuel loading pattern (B-1)

1. Aluminum structure
2. LVDT
3. LVDT connecting rod
4. Coils
5. Aluminum block
6. Aluminum rod
7. Cadmium (absorber)

(a)   (b)
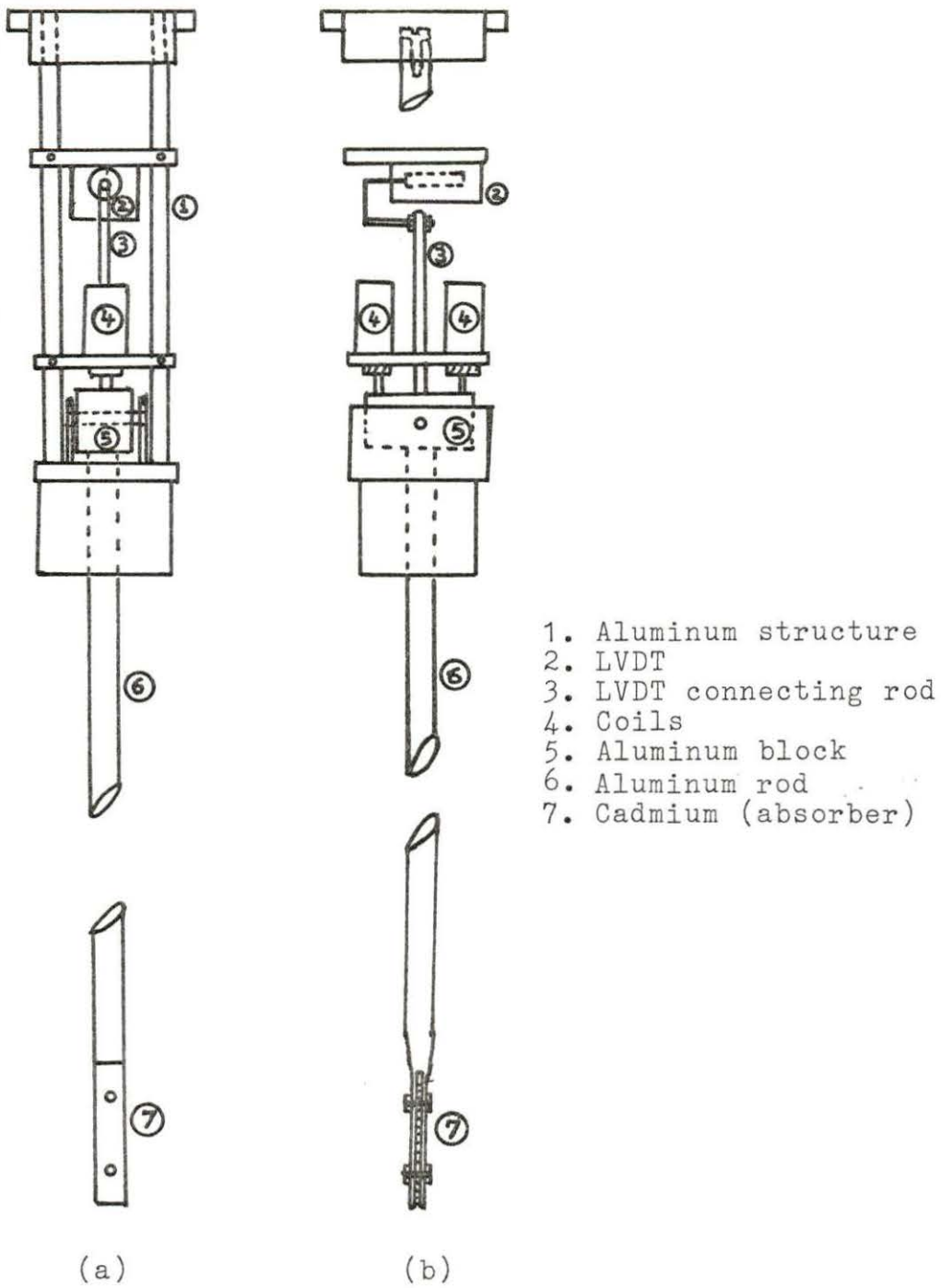
Figure 4.5. Front and side views of the
             vibrator assembly

1. Mounting plate
2. Teflon screw
3. Tightening plate
4. Vibrator thimble
5. Detector thimble
6. Plastic screw
7. Fuel element
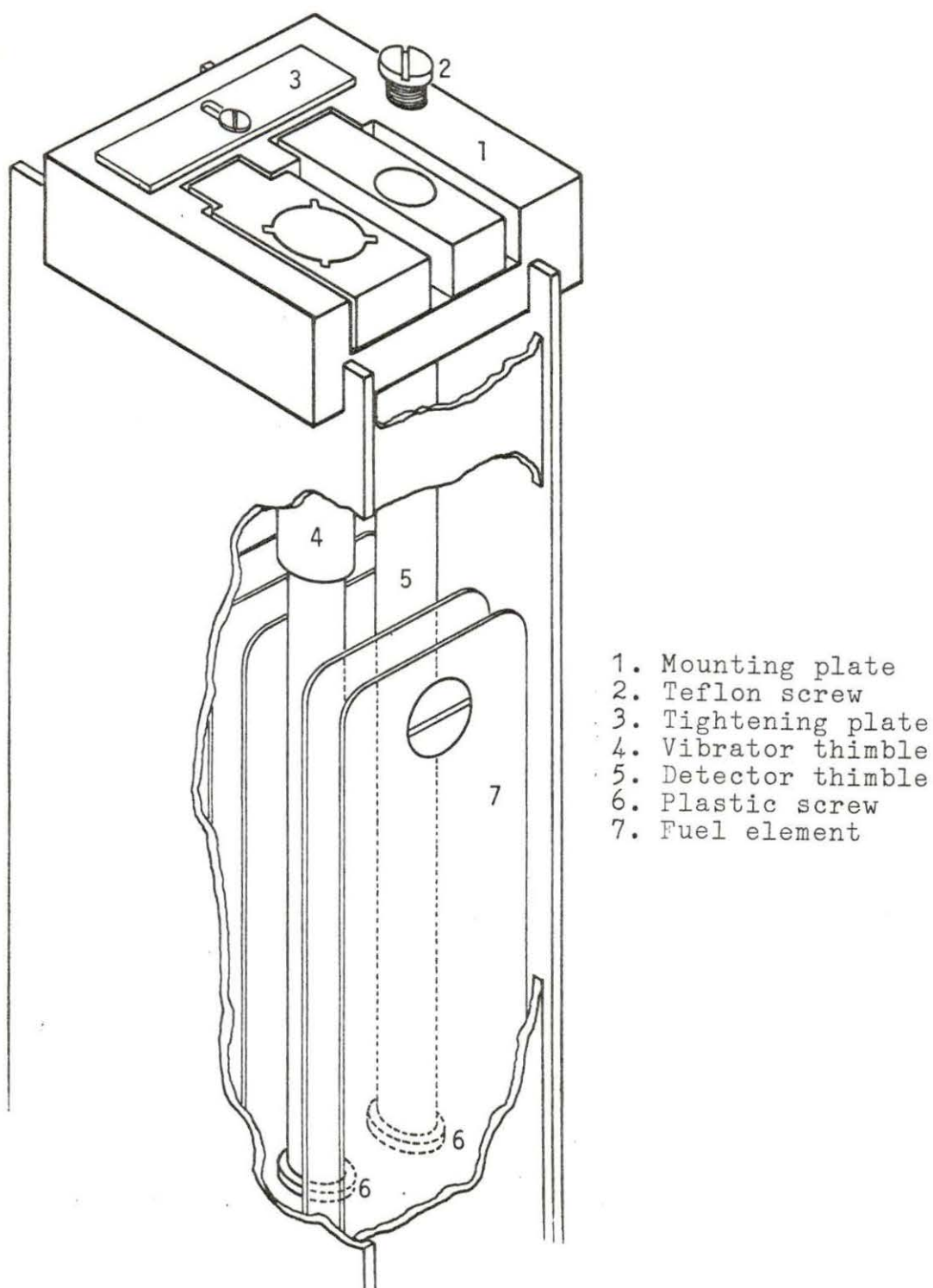
Figure 4.6. The vibrator assembly-core tank configuration

(vibrator enclosure) which is located in the space between
the fuel plates of the modified assembly in S-2 with the
third plate removed (Figure 4.6). A plastic screw at the
bottom end of the thimble can be tightened to make the
tube water-tight for 'dry' operation or opened slightly to
fill the tube with water. The normal position of the
absorber is at the mid-elevation of the fuel element. The
vibrator assembly can be rotated ninety degrees resulting
in two possible planes of vibration, one parallel to (EW)
and the other perpendicular to (NS) the fuel plates.

Another aluminum thimble (detector enclosure) located
about 3.8cm from the vibrator enclosure holds a 3-inch x
5/8-inch diameter BF_3 detector (Figure 4.6). The space in
this tube is filled with Plexiglas 'donuts' which have
approximately the same neutronic characteristics as water.
The vibrator and detector thimbles are held in place by
a mounting plate resting on top of the separator plates
of the core tank. When the vibrator is on the east side,
it is located about 10.6cm, and the detector is located
about 14.4cm, from the north-south center line of the reactor.
One of the limitations of the whole apparatus is that due
to space limitations only one detector can be located in
the core. Ideally, one would like to have a detector on
either side of the vibrator to study the local-global
interaction. This was accomplished by interchanging the

positions of the detector and absorber, but this requires
two experimental runs to get one complete set of data.
The cables come out of the reactor through special shield
plugs as shown in Figure 4.2.

Two 24-volt DC (Guardian model TP 3.5 x 9) push type
coils are used in the apparatus. Figure 4.7 shows the coil
driving system. The coil switching unit (constructed by
the ISU Engineering Research Institute Electronics Shop)
electronically switches power from a DC power supply
between the two coils at the frequency of the input to it.
Two types of driving signals (input) were used; one is a
pseudo-random binary sequence (PRBS) from a noise
generator (HP model 3722A) with the clock frequency
supplied by an external square wave generator. The
second type of driving signal used was a single frequency
square wave from a signal generator (Wavetek model 111).
Due to electrical and magnetic coupling the signal cable
was susceptible to noise pickup from these coils. The
reduction of noise pickup is dealt with in Appendix A.

The movable core of the LVDT (Schaevitz model 100MHR)
is attached to the vibrating absorber (Figures 4.5a and
4.5b). The magnetic coupling between the primary and the
secondary of the linear transformer depends on the position
of the core inside the hollow cylindrical transformer.
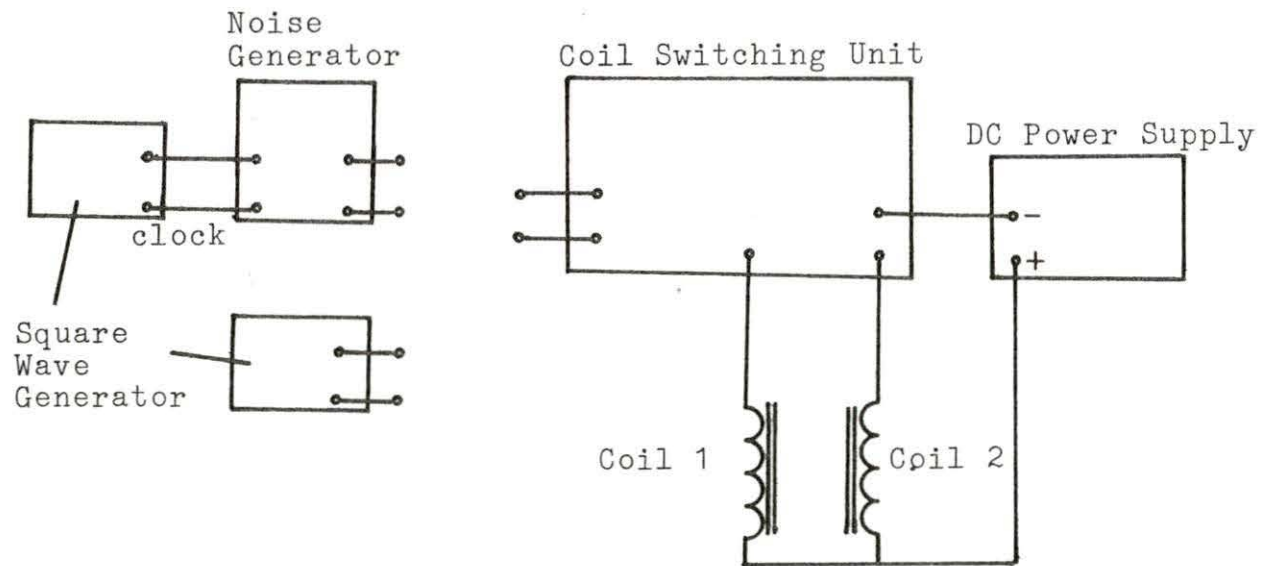
Figure 4.7. The coil driving system

The primary excitation signal is provided by a signal
conditioner (Schaevitz model LPM210). The AC output of the
LVDT is demodulated by the signal conditioner to
get a DC voltage which linearly corresponds to the
position of the core and the position of the absorber.

3. Data acquisition and analysis system

The data acquisition and analysis system is shown in
Figure 4.8. One of the three channels of data available
was from the LVDT through the signal conditioner which
provides information regarding the position of the
absorber. The other two channels of data were from two
detectors which monitor the flux perturbation produced
by the absorber motion.

One of the detectors was an in-core detector (D_1)
located about 3.8cm from the absorber. This is a BF_3
detector (N. Wood model G-5-3, 60cm of Hg gas pressure)
operating in the ion-chamber mode. The high voltage of
about 270 volts is supplied by batteries. Note that the
negative side of the battery is connected to the central
electrode of the detector. The signal is taken from the
detector casing (negative side). This arrangement would
result in a phase shift of 180° between the reactor
power level and the detector output because an increase
in reactor power produces a negatively increasing detector

1. LPM210 Signal Conditioner
2. Preamplifier
3. Picoammeter
4. High voltage (270 volts)
5. Compensating voltage (50 volts)
6. High voltage (600 volts)
7. High pass filter
8. Low pass filter
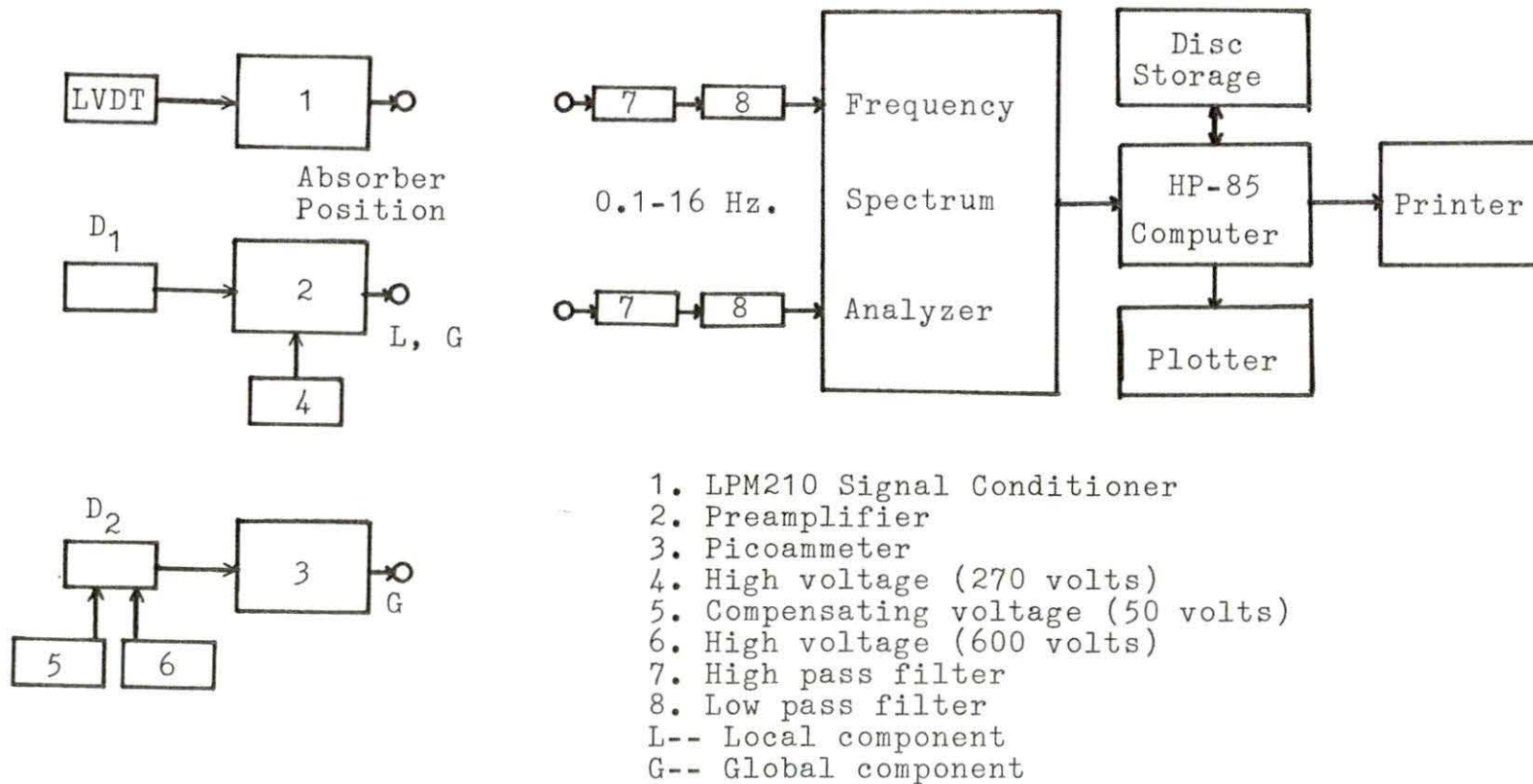L-- Local component
G-- Global component

Figure 4.8. The data acquisition and analysis system

signal. The detector was covered with aluminum foil to provide shielding (see Appendix A). The current output from the detector is fed into a DC-coupled preamplifier (Ames Laboratory model 1616) which converts the detector current to an output voltage. The phase between the input and output signal is almost zero. Three levels of gain setting can be selected on the preamplifier. The saturation characteristics of the preamplifier were investigated previously (5) and the output saturates at about twelve volts.

The second detector (D_2) was a compensated ion chamber (CIC, Westinghouse type 6377) located in the position of the 19-inch stringer in the thermal column, at a distance of about 35cm from the vibrator when fully inserted (Figure 4.1). The high voltage and the compensating voltage used were about 600 volts positive and 50 volts negative, respectively. In this case, the positive side of the high voltage was connected to the center electrode and the output was taken from the casing, the positive side, and the reactor power and the detector signal are in phase. The detector current was measured using a high-speed picoammeter (Keithley model 417) which was capable of giving an output voltage between zero and minus three volts for a meter deflection of zero to full scale on any range. This introduces a phase shift of 180° between the input and the

output of the picoammeter. There is provision on the picoammeter to buck out the DC value of the current.

At any time, it was possible to analyze any combination of two out of the three channels of data available. The signals passed through two identical band-pass filters. Each band-pass filter was formed by a second order Butterworth low-pass filter (Burr-Brown model UAF11) with a cut off at about 16 Hz and a fourth-order Butterworth high-pass filter (Krohn-Hite model 3321) with a cut off at 0.1 Hz. The pass-band was sufficient to collect data in the frequency range of interest but eliminated both the DC-component and the high frequency noise which would prevent operation with high sensitivity settings on the frequency spectrum analyzer.

The signals from the filters were fed into a two channel frequency spectrum analyzer (HP model 3582A) which uses the fast Fourier transform (FFT) based digital algorithm. From the time signals, the instrument is capable of calculating the magnitude of the frequency spectra (square root of the APSD), and the phases for the two input signals, the transfer function magnitude and phase between the two channels, and the coherence between the two channels. These data were stored on disk for later processing with a microcomputer (HP 85) interfaced with

the analyzer. Procedures similar to the ones described in
reference (5) were used to store and later retrieve and
analyze the data using the microcomputer. It was necessary
to modify or rewrite some of the programs copies of which
are given in Appendix B. Plotting of the data was
accomplished through the use of a digital plotter (HP 7225A)
interfaced with the computer.

B. Pre-experimental Procedures

An experimental plan, including the safety analysis
report (34), was prepared for the experiment. This was
approved by the Reactor Use Committee, and the pre-
experiment tests were performed as outlined in it. The
first step involved testing the fuel assembly to be used
in the experiment for fission product leakage. The
assembly was found to show no leakage, and it was
modified for the experiment by removing the third fuel
plate and substituting spacers of equal thickness. This was
done according to the procedure written by Hennessy (35) and
approved by the Reactor Use Committee.

Next the modified assembly (N3H-AM) was put in the
experiment location S-2. As mentioned previously, the
original fuel loading was rearranged to get enough excess
reactivity for the experiment. The final loading pattern

B-1 (2978gm) is shown in Figure 4.4; the excess reactivity
was $0.52 at 80F. The static worth of the experiment was
about $0.25, and that of the CIC in the thermal column was
about $0.08. The dynamic reactivity was found to be not
more than $0.01. For more details, see reference (36).

It is worth mentioning that the all aluminum
construction of the apparatus and the casing of the detector
significantly reduced the problem of residual radioactivity.

C.   Experimental Procedures

The location of the modified assembly, the experimental
apparatus and the in-core detector (D_1) are shown in Figure
4.1. As mentioned previously, the vibrator-detector positions
could be interchanged. The detector in the core could be
located on the east or west side of the absorber.
Measurements could be taken with the vibrator moving in
either the east-west (EW) or the north-south (NS) direction.
The three letter designation, for example "E EW", describes
the detector position as east and the direction of absorber
vibration as east-west. A second detector (D_2) was located
in the thermal column. The various possible detector
locations and directions of vibration are shown in
Figure 4.9.
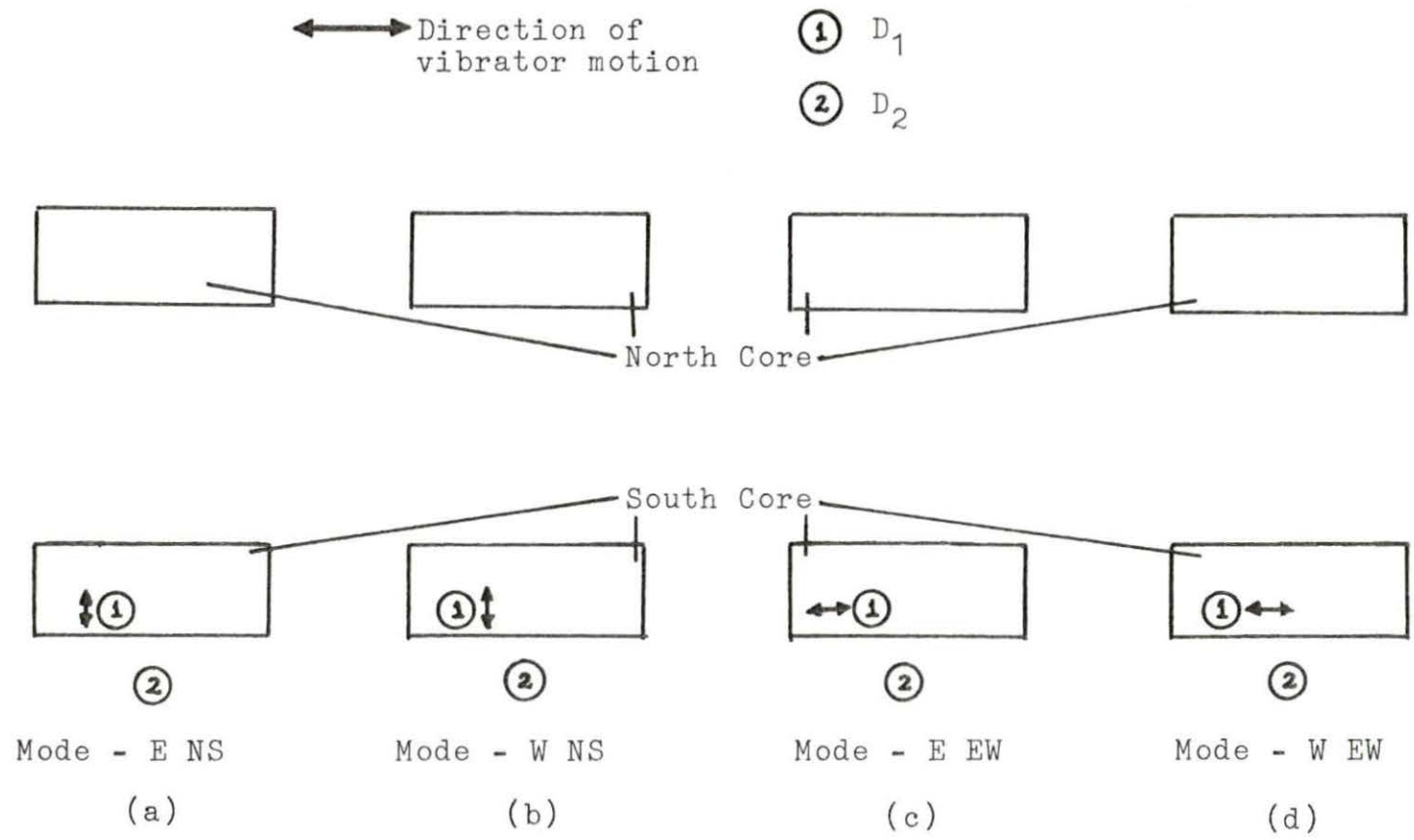
By flooding the vibrator thimble, it was possible to

Figure 4.9. Possible combinations of detector locations and direction of vibrations of the absorber

change the magnitude of the flux gradient in the region
in which the vibrator was moving. Two cases, thimble
flooded and thimble unflooded, were investigated. Another
way of changing the flux gradient is by changing the
regulating rod positions. Measurements were done with the
regulating rod at 0% and at 100% withdrawn to see if flux
gradient effects could be observed.

Two types of signals were used for the vibrator
excitation; the PRBS signal and the 1.5 Hz square wave.
With a clock frequency of 18 Hz and a sequence length of
1023, the noise generator produces a complete spectrum of
input frequencies from zero to twelve Hz with an amplitude
of 10 volts. The range of practical interest was restricted
to the frequency range of 0.08 to 4 Hz. The upper limit
was imposed due to the fact that above this value the
vibrator response falls off rapidly. Figure 4.10 shows
the frequency spectrum (APSD) of the absorber motion as
registered by the LVDT for the flooded and unflooded
case. The vibrator response falls off at a
lower frequency for the flooded case because of the
increased damping effect of the water. The 1.5 Hz square
wave serves as a single driving frequency (the harmonics
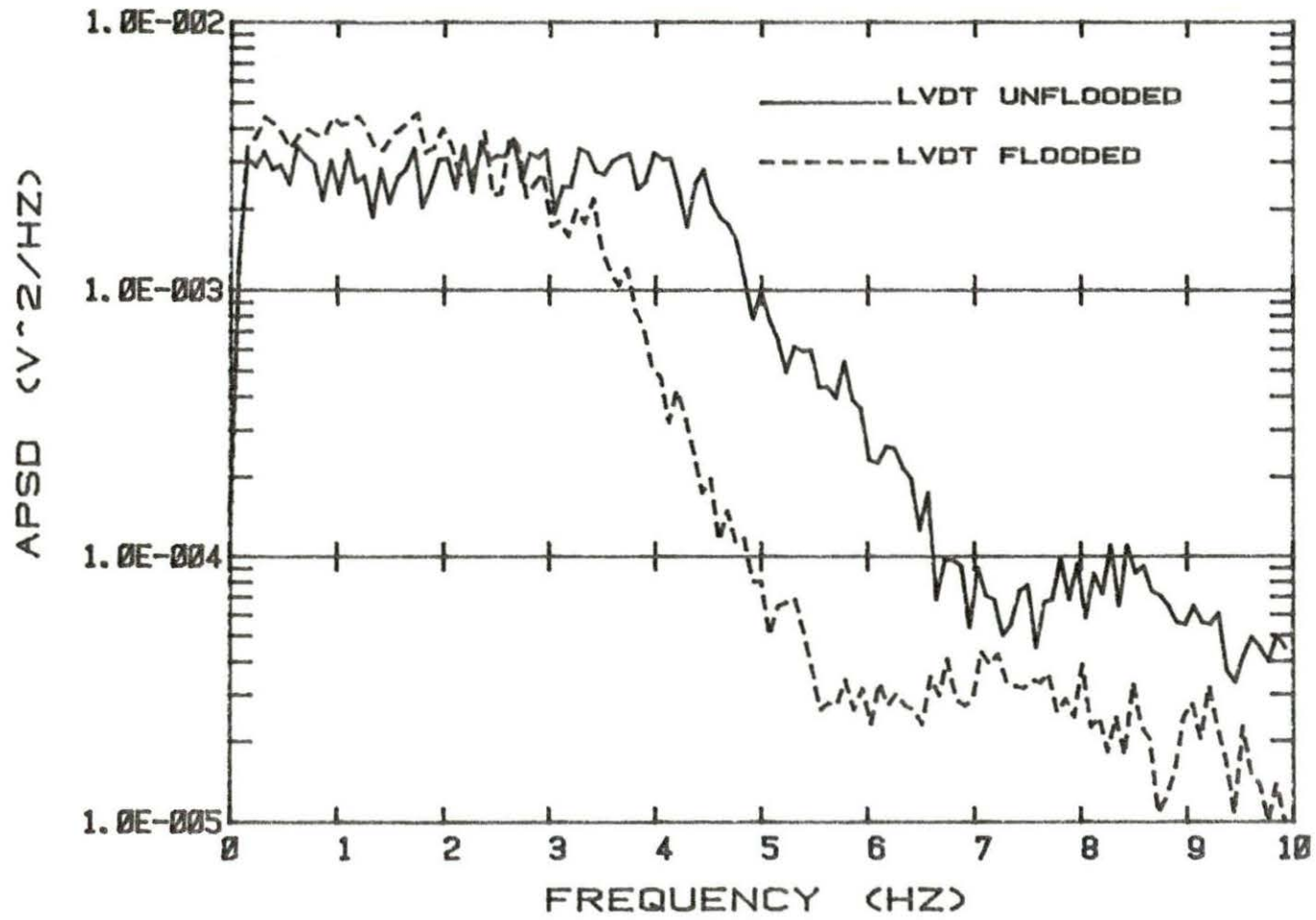are also excited but to a lesser degree). The vibrator

Figure 4.10. The APSD of the LVDT output for a PRBS input

motion, and hence, the detector signal are much stronger than for the PRBS input since the signal power is concentrated at one frequency rather than spread over a range of frequencies as in the case of PRBS input. Figure 4.11 shows the APSDs of the absorber motion for the 1.5 Hz square-wave signal.

Figure 4.12 summarizes the various operational modes in which the experiment was performed. Only one complete branch is shown in the figure. D_1 and D_2 data along with the LVDT data were collected for all possible modes.

As mentioned before, for each experimental situation three channels of data, viz. LVDT, D_1 and D_2, were available. For the different combinations of these three, five sets of data (the square root of the APSDs for the two channels, the transfer function magnitude and phase, and the coherence between the two channels) were measured. For the 1.5 Hz signal it was sufficient to take only eight rms averages with the analyzer, but for the case of the PRBS input a higher number of averages (16 or 32) were necessary since signals were weaker and subject to more statistical variation. For all the runs, the reactor power was 200W and the coolant inlet temperature was 80F. The reactor was operated manually and the data
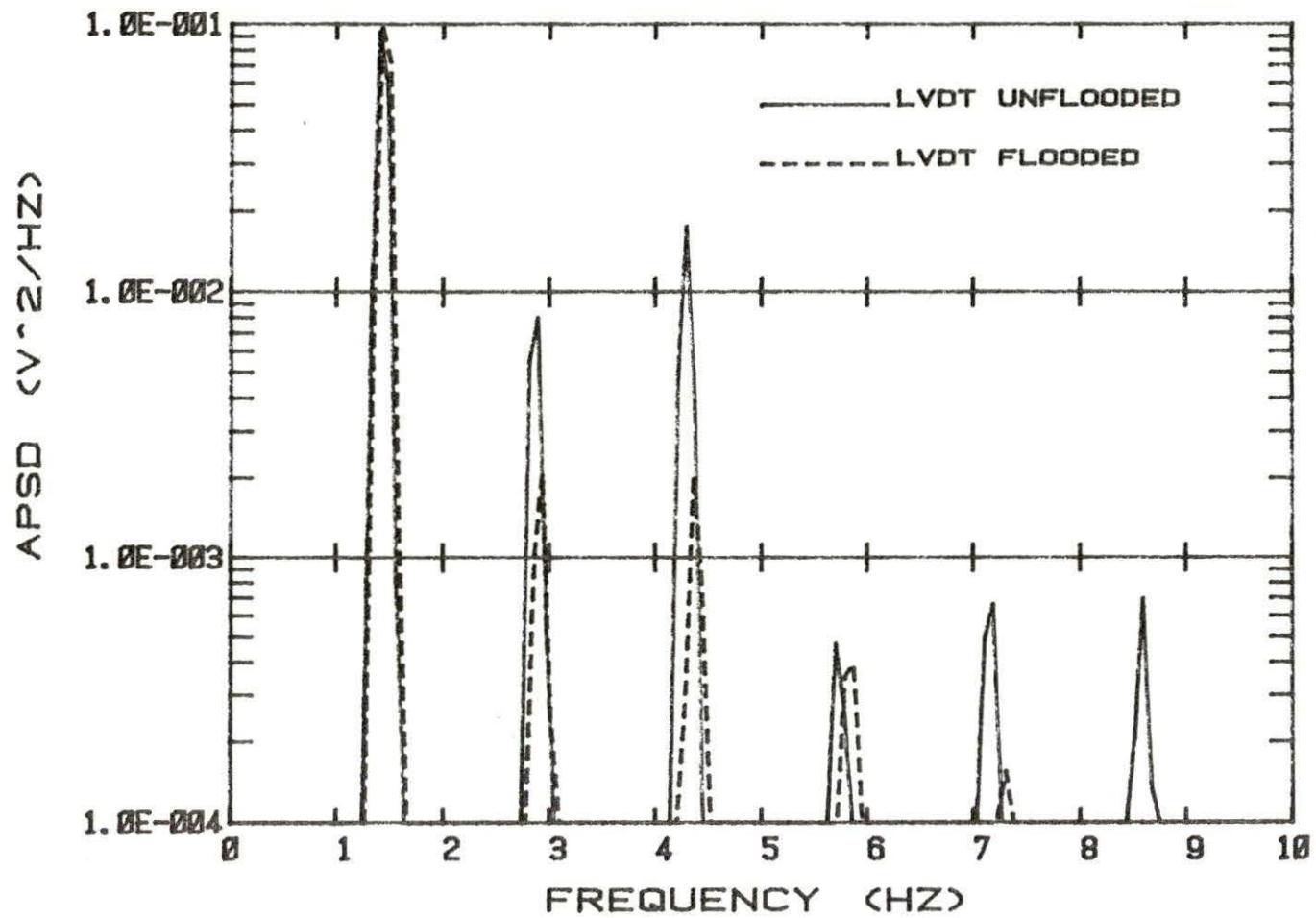
Figure 4.11. The APSD of the LVDT output for 1.5 Hz square-wave input

```
Vibrator environment  -------------------                    Unflooded        Flooded

Vibrator motion       -------------------           EW       NS

D₁ (vibrator) location  -----------        E(W)      W(E)

Position of Reg. rod  --------     0%      100%

Vibrator input signal ----  PRBS      1.5 Hz.
```
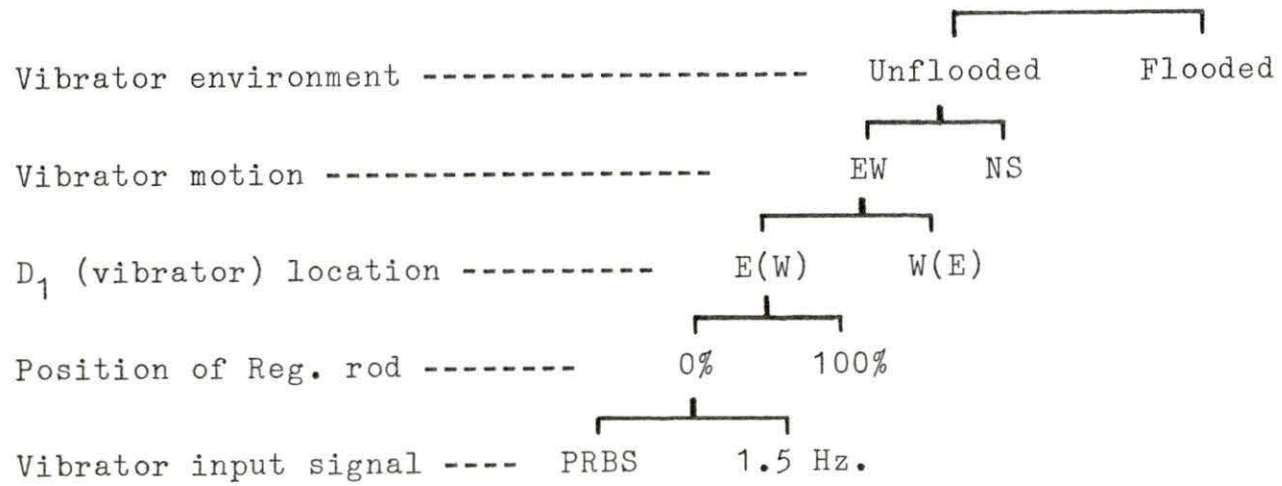
Figure 4.12. Summary of the various operational modes

were collected during the time the reactor power was not
drifting. With the automatic power controller on, the
detector APSD was observed to show a peak at about 0.16 Hz
corresponding to the automatic controller feedback
frequency. The sensitivity of the analyzer was adjusted
to the maximum without overloading. The analyzer and the
filters were zeroed before data collection to reduce
the DC component that appears at the analyzer input.

V. DISCUSSION OF RESULTS

The data collected as described in the previous
section were processed by the spectrum analyzer to
calculate the square root of the APSDs of the two inputs
to the analyzer, the transfer function magnitude and
phase, and the coherence between the two inputs. These data
were stored on disk for each run. It was observed that,
due to design limitations, the LVDT frequency spectrum
varied slightly for the different runs. In order to correct
for this, and to compare the data from different runs, it
was necessary to normalize the data. The raw APSD for each
detector signal was corrected for background (neutron noise
at the operating power of 200W without the vibrator
operating) and normalized to the LVDT APSD to produce a
normalized APSD as follows:

$$APSD_{normalized} = \frac{APSD_{signal} - APSD_{noise}}{APSD_{LVDT}} \qquad (5.1)$$

Figures 5.1 and 5.2 show the raw APSD of the signal and
the background noise from D_1 and D_2 for a typical run.
The solid line plots in Figures 5.3 and 5.4 show the
normalized APSD for D_1 and D_2 data obtained using
equation 5.1 and data from Figures 5.1 and 5.2. In the
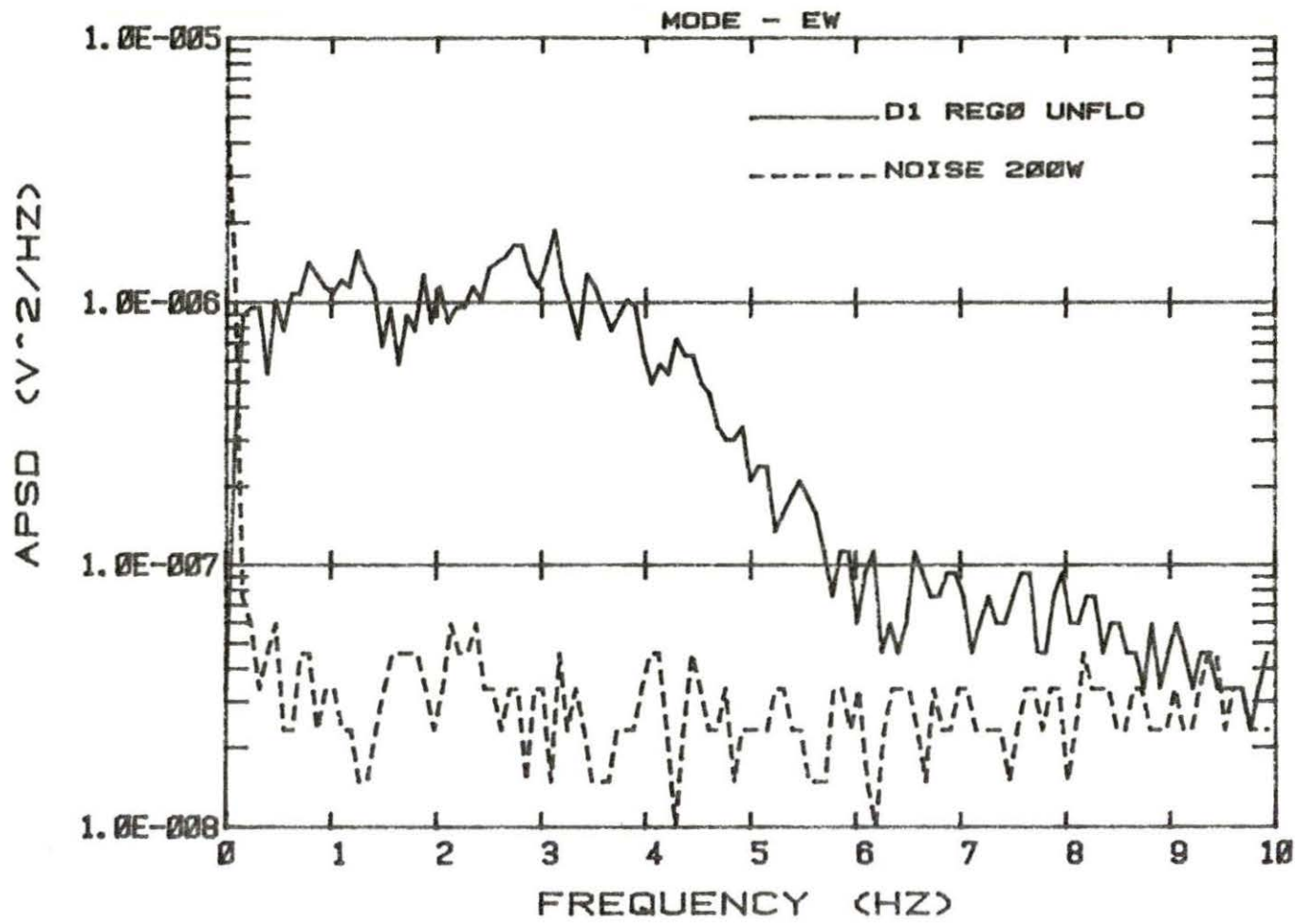
Figure 5.1. D_1 APSD with PRBS input signal and reactor background noise at 200W
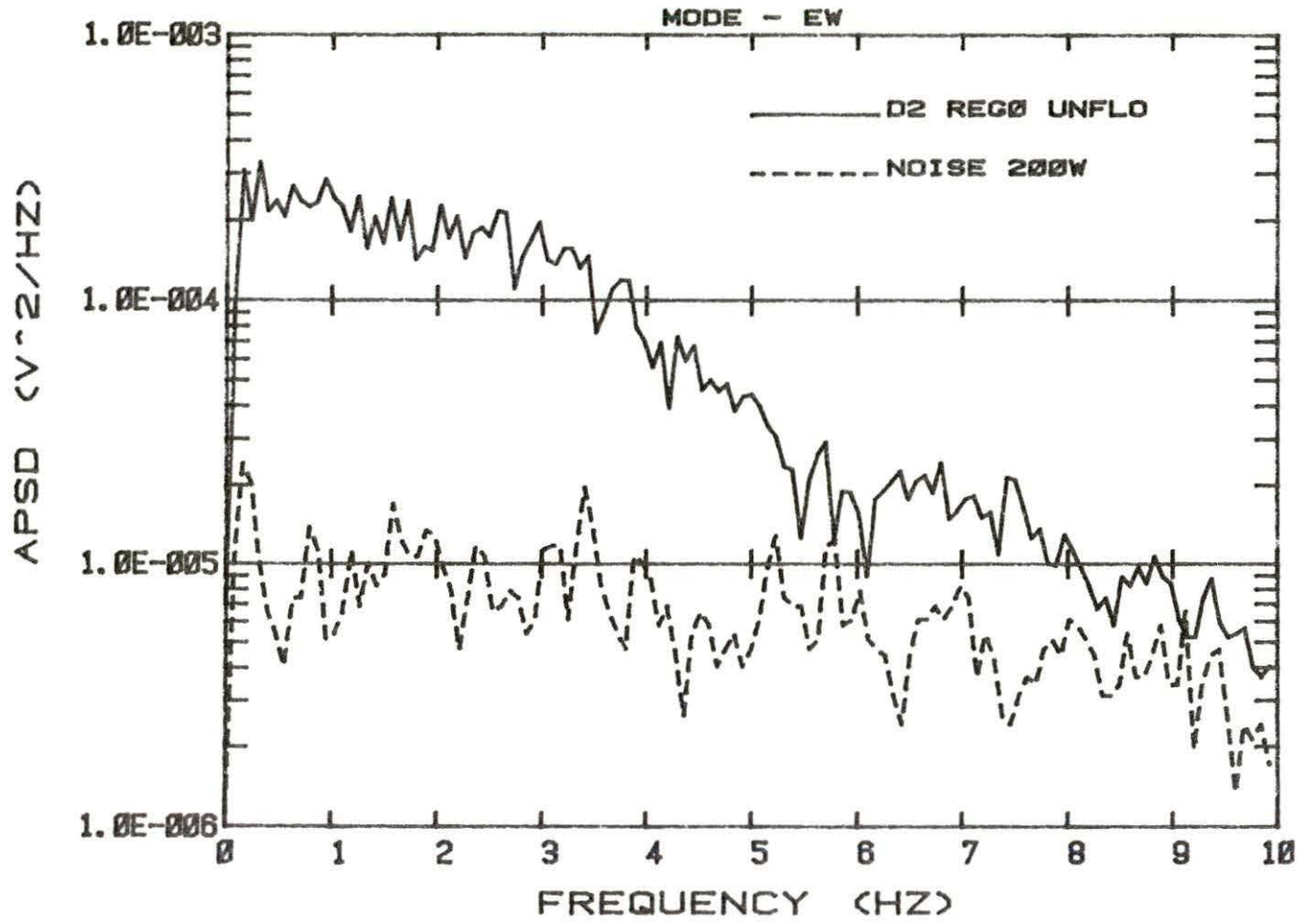
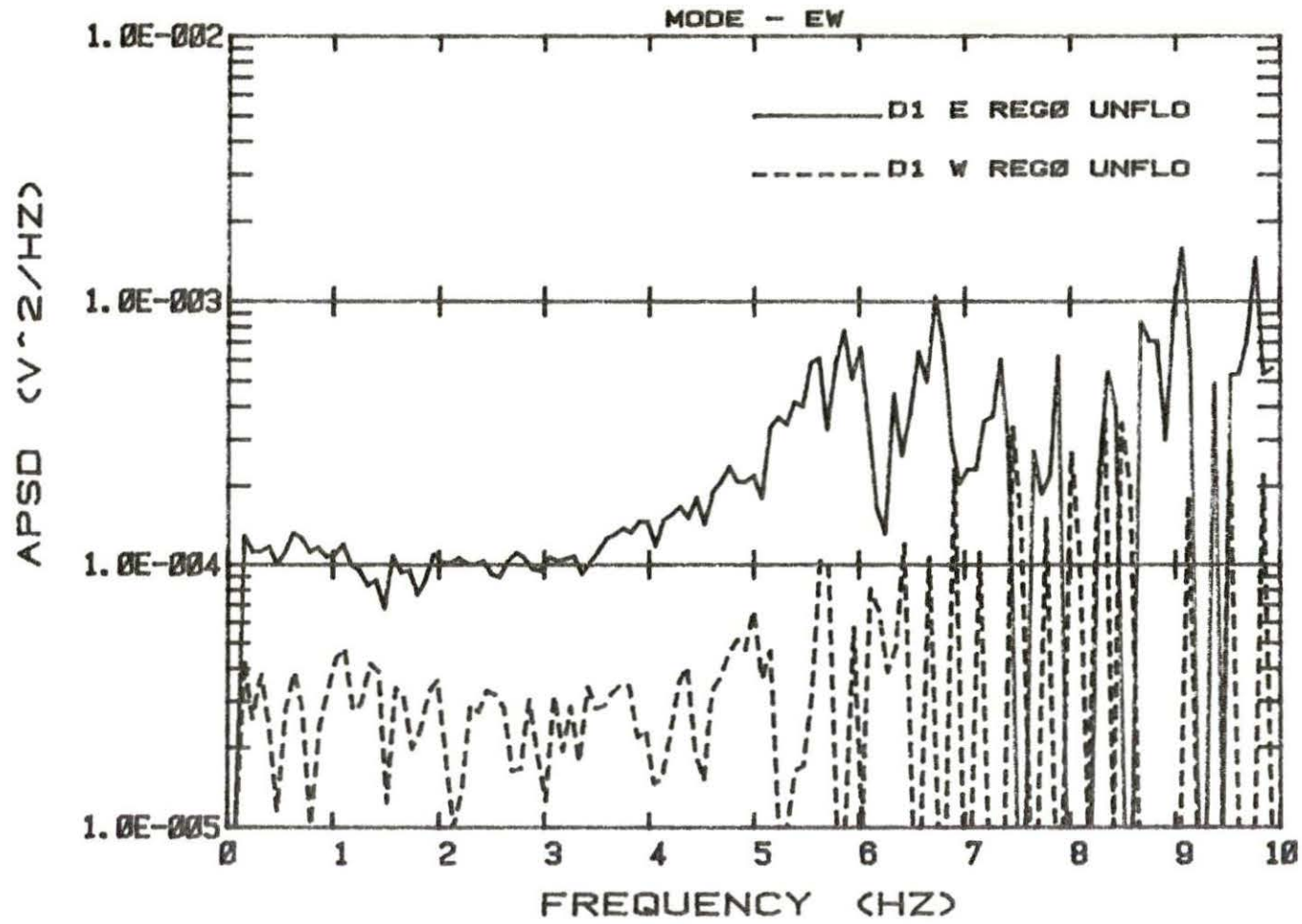Figure 5.2. D$_2$ APSD with PRBS input signal and reactor background noise at 200W

Figure 5.3. Normalized APSD of D_1 on the east and west side of the
absorber for a PRBS input signal, thimble unflooded
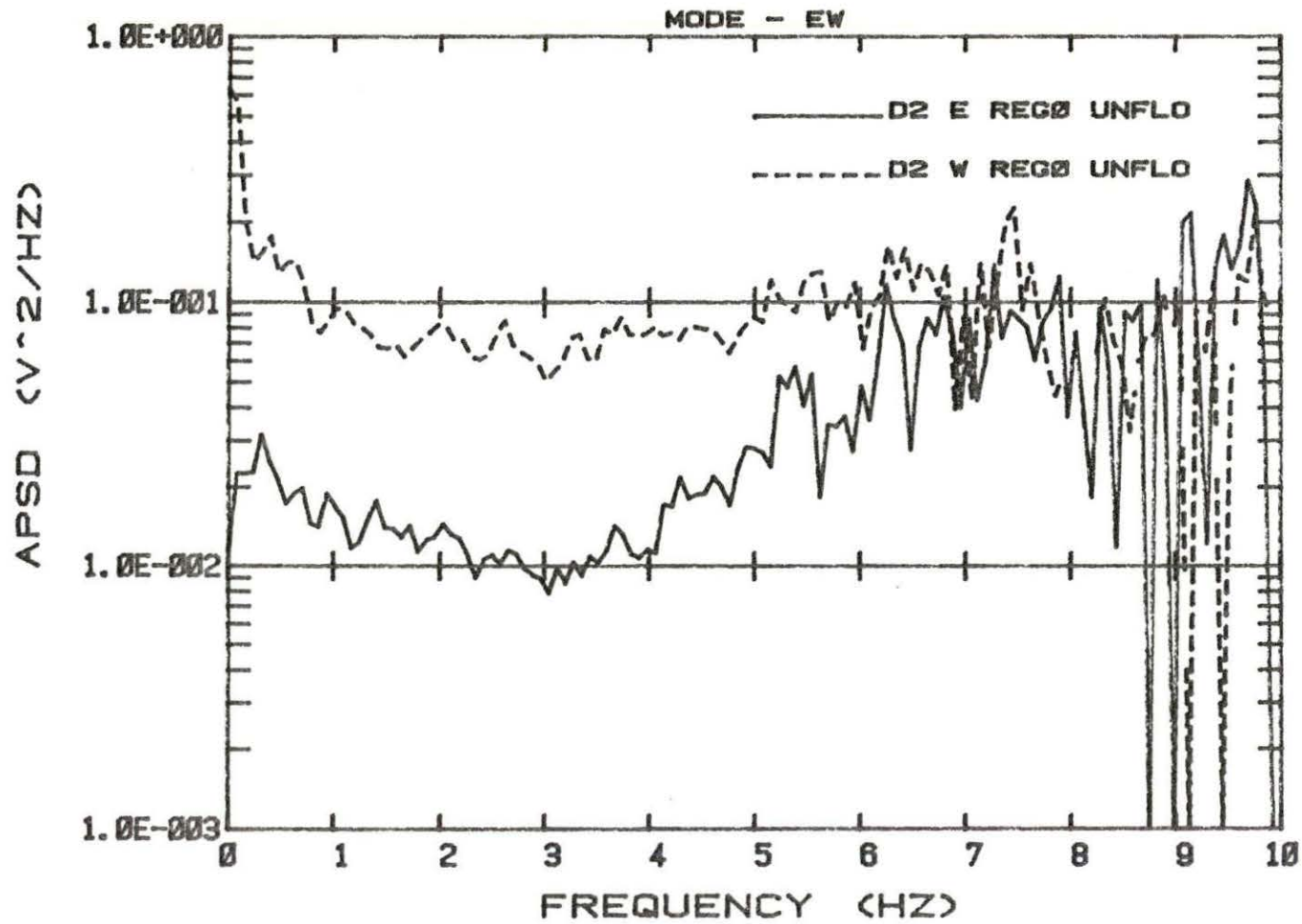and regulating rod at 0%

Figure 5.4. Normalized APSD of D_2 for the two locations of the absorber, for a PRBS input signal (E and W corresponds to D_1 position)

plots showing the detector responses to a PRBS input, the region above 4 Hz may be discarded since as seen from Figure 4.10 it is clear that the vibrator response falls off rapidly above this frequency. The case of EW (Figures 4.9c and 4.9d) vibration with the detector on the east and west side will be discussed first, since this shows the effects of the local-global interaction. Based on the assumption that there is a positive flux gradient from west to east, the local and global components will add on the east side and they subtract on the west side.

A. EW Vibrator Motion

Four different cases (see Figure 4.12) can be investigated for this mode of vibrator motion for the two types of excitation signals. They are vibrator thimble unflooded (UNFLO) and flooded (FLO) with the regulating rod position at 0% (REG0) or 100% (REG100) out. Figures 5.3 and 5.4 show the normalized APSDs for the detectors D_1 and D_2 with PRBS excitation for the case of the thimble unflooded. For both figures, the regulating rod was positioned at 0% out. The E and W in the legend of Figure 5.3 and 5.4 indicate the position of D_1. Note from Figure 4.9 that if D_1 is on the east (E), the vibrator will be positioned on the west (W) side and vice versa.

The two curves in the above figures are for the cases of D_1 on the east (D1 E) and on the west (D1 W) side of the absorber. From Figure 5.3, it is evident that the local and global components add on the east side and they subtract on the west side. The APSD for D_2 (Figure 5.4) is higher when the vibrator is on the east side. In this case, the absorber is closer to the center of the reactor and is in a higher flux region resulting in a higher reactivity (negative) input.

In the discussion above, it was assumed that there is a positive flux gradient from west to east. This can be proved as follows. The transfer function phases between D_2 and the LVDT for D_1 on the east and on the west side of the absorber are shown in Figure 5.5. This figure provides information which can be used to establish the phase relationship between the LVDT signal and the actual reactivity input to the reactor. This reasoning is based on the assumption that D_2 sees only the global part of the response. To develop this analysis, assume that a positive flux gradient exists from west to east in the experiment region, and therefore, the negative reactivity input increases as the absorber moves to the east. It was observed that when the absorber moves to the east the LVDT signal decreases. This implies that a negative
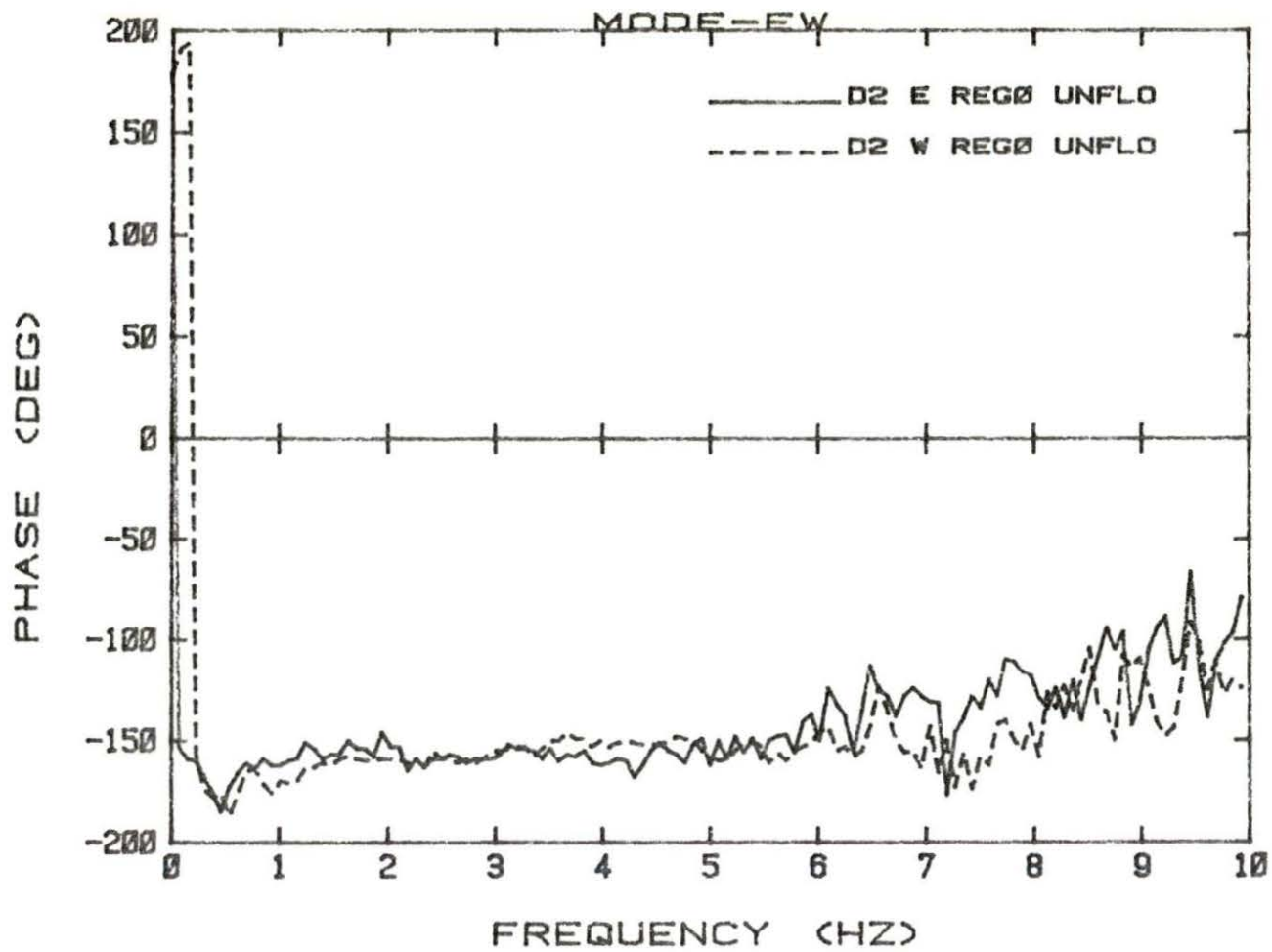
Figure 5.5. The transfer function phase between the LVDT and D_2 when D_1 is on the east and west side of the absorber, for a PRBS input signal

reactivity insertion corresponds to a decreasing LVDT
signal (in phase). The global component of the detector
response decreases because of the increased negative
reactivity. The signal from D_2 decreases, but the
picoammeter introduces a 180° phase shift. Therefore,
even though the reactivity (global) component is in phase
with the LVDT, D_2 and the LVDT will be out of phase (180°).
In reality the global effect lags the reactivity input by
the phase angle determined by the point reactor transfer
function which, in this frequency range, is about 10-15
degrees. Therefore, the phase between D_2 and the LVDT is
about 180 - (10 to 15) degrees. Figure 5.5 confirms this
reasoning and supports the assumption that the flux
gradient is positive from west to east.

The phase relationship between the various components
of the detector response are illustrated in the phasor
diagram of Figure 5.6. In constructing the diagram, the
local effects were assumed to be real and the LVDT signal
was taken as the reference vector. Clockwise is taken as
the positive direction. The global component 'G' lags the
LVDT signal, and as explained before, the thermal column
detector (D_2) response is out of phase with G. As the
absorber moves towards the east the LVDT signal, as well
as the local component seen by D_1 located on the east,
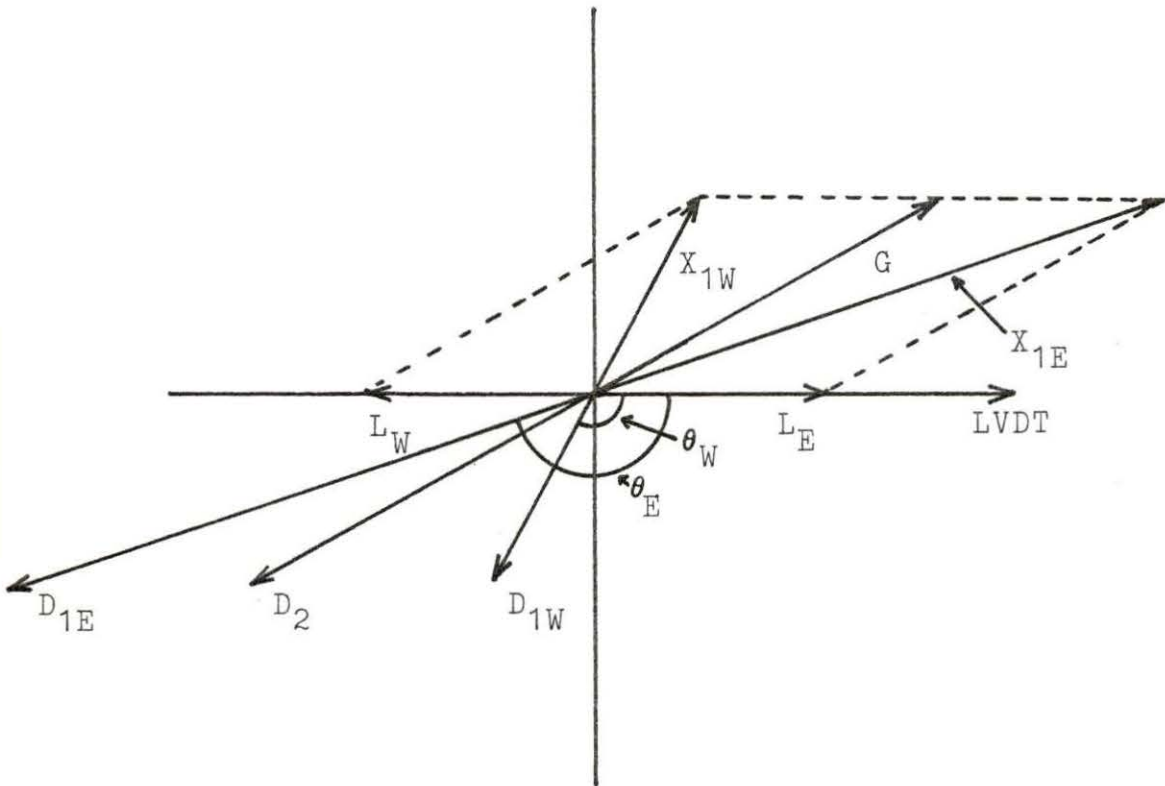
G-- global component (Note that $G=G_{1E}=G_{1W}=G_{2E}=G_{2W}$ are
    in phase, but the magnitude is different)
L-- local component
X-- resultant reactor response
D-- resultant detector response accounting for instrument
    phase shift

Figure 5.6. Phasor diagram showing the relation
             between the local and global components

L_E, decreases. Therefore, L_E is in phase with the LVDT signal, while L_W, the local component seen by the west detector, is out of phase with the LVDT signal. The global component seen by D_1 on the west, G_{1W}, and by D_1 on the east, G_{1E}, have the same phase relationship with the LVDT as that of the signal from D_2, but the magnitudes are different. The resultant of L_E and G_{1E} is X_{1E} and that of L_W and G_{1W} is X_{1W}. This resultant is the flux response seen by the detector D_1. Since the signal is taken from the negative side of D_1, there is a 180° phase shift between the reactor (or flux) response and the detector output (i.e. between the X and D in Figure 5.6). The preamplifier does not introduce any significant phase shift. The responses of the detectors supplied to the analyzer are shown as D_{1W} and D_{1E}, respectively. The phase difference between D_{1E} and the LVDT, θ_E, and D_{1W} and the LVDT, θ_W, are values measured by the spectrum analyzer. Note that if L_W is greater than G_{1W} the angle θ_W will approach zero with an increasing L/G ratio.

Figure 5.7 shows the transfer function phase between D_{1W} and the LVDT and between D_{1E} and the LVDT for the case being discussed. The analyzer uses input A as reference while calculating the transfer function phase. While collecting the data the LVDT signal, which is used as the
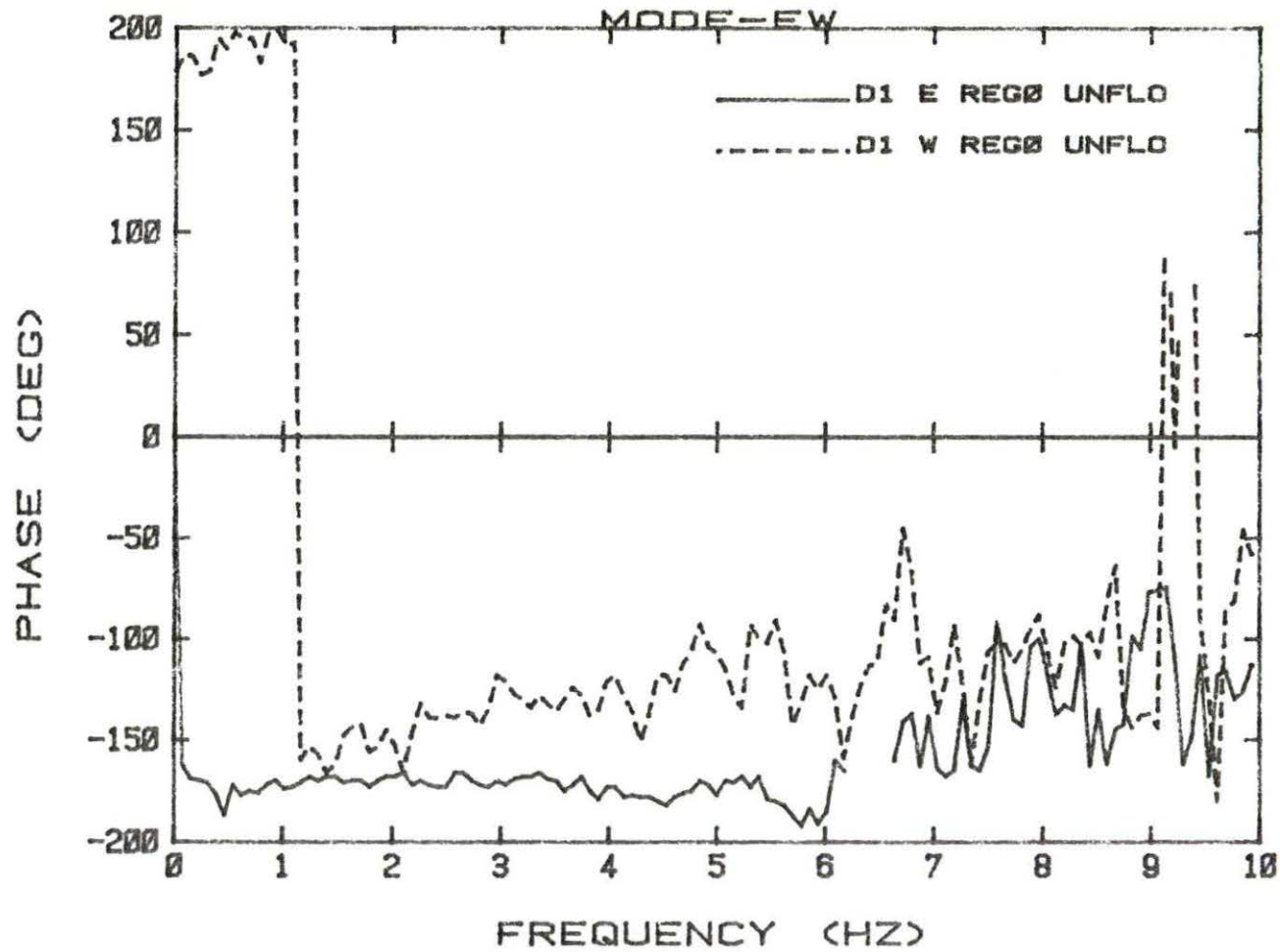
Figure 5.7. The transfer function phase between the LVDT and D_1 on the east and west side of the absorber, for a PRBS input signal and the unflooded case

reference input in the phasor diagram (Figure 5.6), was connected to input B. Therefore, even though from the phasor diagram the measured phase angle appears to be positive the analyzer calculates it as a negative angle. This explains the negative angles in all phase plots. The phase between D_{1W} and the LVDT is closer to 180° than it is to 0° and implies that G_{1W} is greater than L_W. The flipping of the plot from -160° to 200° (360° difference) is due to instrument limitation. At this stage, equations 3.17 through 3.20 were used to calculate the local to global ratios, L_W/G_{1W} and L_E/G_{1E}. $G_{1W} > L_W$ implies that L_W/G_{1W} is less than one. Also note that θ_E is approximately 170° and X_{1E} lies along the bisector of the angle between L_E and G_{1E} ($D_{2E}/$LVDT phase is $\approx 160^{\circ}$) which implies that L_E/G_{1E} is close to one. Of the two possible values for the two L/G ratios, the numbers that satisfy the above conditions were chosen. These values are shown in Table 5.1. For the PRBS case, the frequency range between 0.8 to 4. Hz was used for the calculations with a value of L/G being calculated for each frequency point obtained from the analyzer. The values reported are averages for all data. The uncertainty in the values of L/G was estimated using the propagation of errors. Note that the relative error in the calculation of the

Table 5.1. Table of local to global ratios for EW vibration

Input Type	Vibrator Environment	Reg rod Position	L/G_{1E}	L/G_{1W}
PRBS	Unflooded	0%	1.3	0.58
PRBS	Unflooded	100%	1.3	0.50
PRBS	Flooded	0%	6.0	3.5
PRBS	Flooded	100%	7.0	3.0
1.5 Hz	Unflooded	0%	1.2	0.68
1.5 Hz	unflooded	100%	1.6	0.60
1.5 Hz	Flooded	0%	2.6	1.1
1.5 Hz	Flooded	100%	3.0	1.5

APSD is given by the square root of the inverse of the
number of averages (32) used by the analyzer to obtain the
APSD. The uncertainty in all the numbers given in Table 5.1
is estimated to be in the range of ± 0.2 to 0.6, the
0.2 is the spread in the L/G value obtained when the
average was calculated for the PRBS case.

The APSDs for the case of a 1.5 Hz excitation, for
the detector D_1 on the west and east side of the absorber,
are shown in Figure 5.8. The position of the regulating
rod was at 0% (REG0) and the thimble was unflooded (UNFLO).
The corresponding plots for D_2 are shown in Figure 5.9.
Note that these plots are not normalized. As in the case
of the PRBS input, the local and global components add on
the east side and subtract on the west side for D_1. Also,
the D_2 plots show the same increased reactivity insertion
when the vibrator is on the east side. Calculations
similar to the one described above were performed to
obtain the L/G ratios shown in Table 5.1. The maximum
values of the peak of the APSD at 1.5 Hz were used for
the calculations. There is a 5-10% difference in the
values of the L/G ratios calculated for the PRBS and
1.5 Hz signal cases. The 1.5 Hz values are assumed to be
more reliable since the signals are much stronger in this
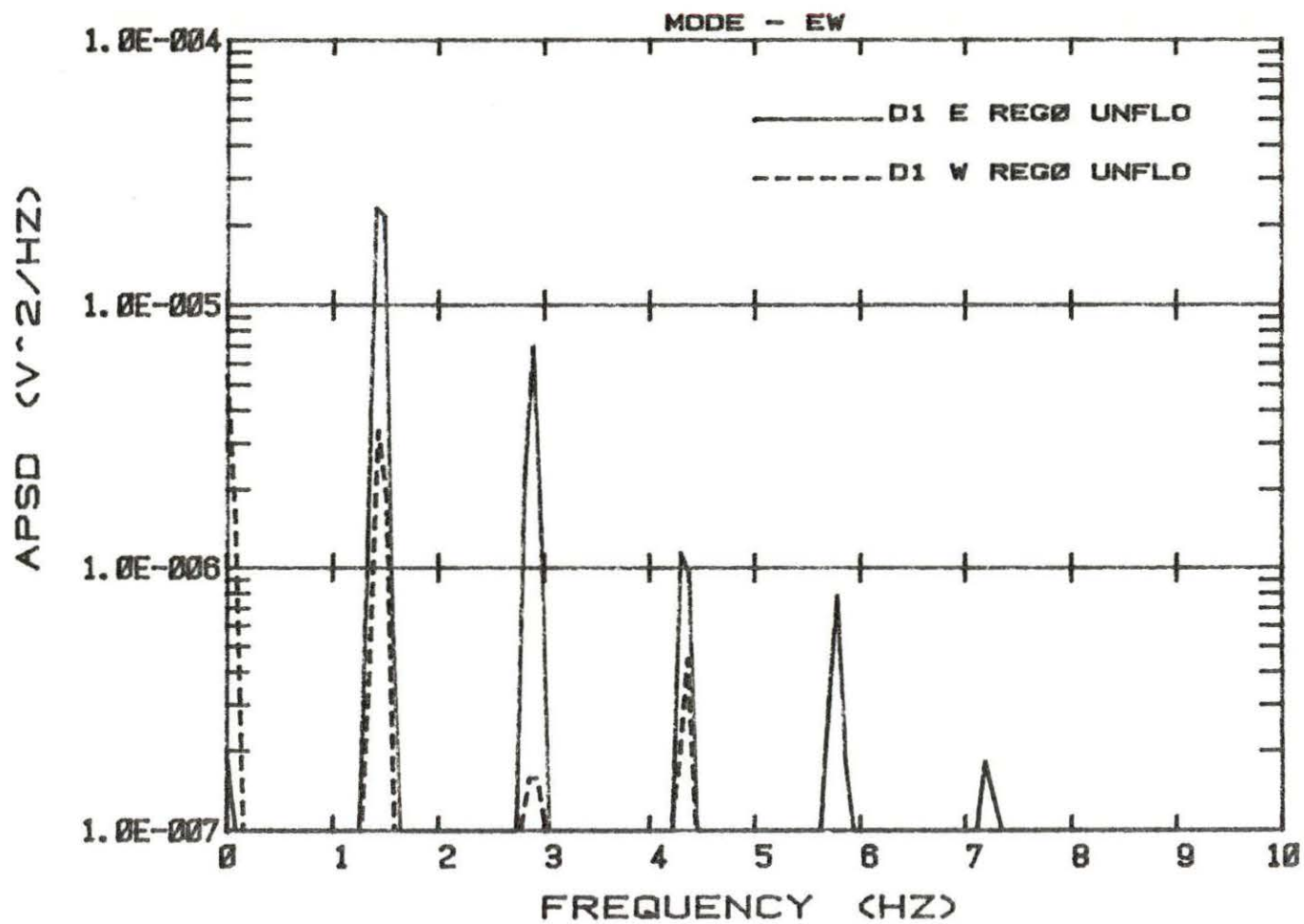case.

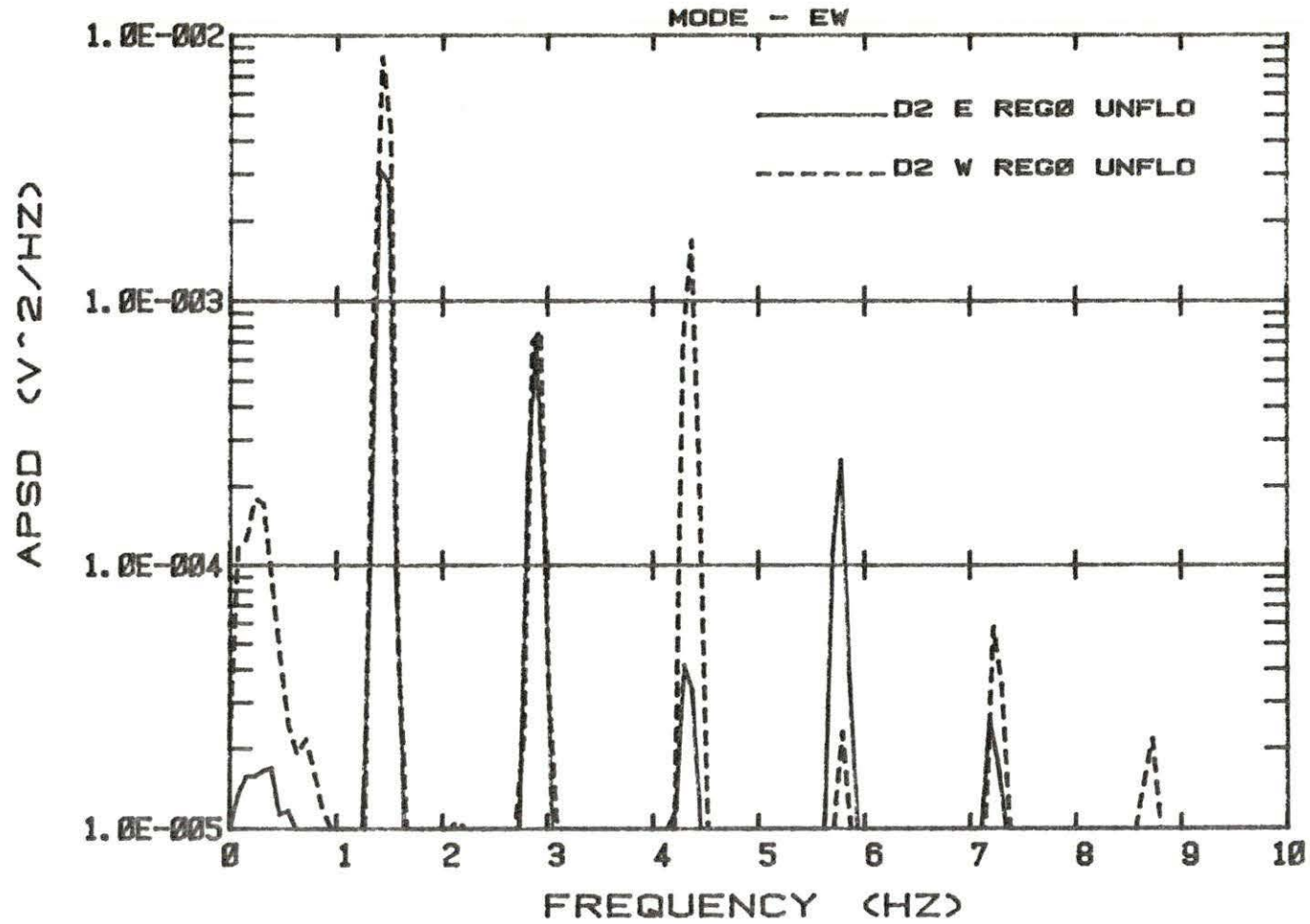Figure 5.8. The APSDs of D_1 on the east and west side of the absorber, for 1.5 Hz input signal

Figure 5.9.   The APSDs of D_2 for the two locations of the absorber, for 1.5 Hz input signal (E and W corresponds to D_1 position)

Measurements were also taken for the case of the regulating rod at 100% (REG100) and the thimble unflooded (UNFLO). The plots (not included) showed a behavior similar to the previous case with the regulating rod at 0%, and no significant change in the response was observed. It was felt that some change might be found because of the change in the flux gradient with regulating rod position change. This lack of change in the response may be due to the fact that the EW flux gradient was not affected significantly by the regulating rod which is positioned on the south side of the experimental set up. The L/G ratios were calculated as before and are shown in Table 5.1. The values for the PRBS and 1.5 Hz cases agreed within 20%.

When the vibrator thimble was flooded for both REG0 and REG100 cases, a significant difference in the detector response was observed. From Figure 5.10, it can be seen that the phase between D_{1W} and the LVDT is close to zero indicating that L_W is greater than G_{1W}, and L_W/G_{1W} is greater than one. The APSD plots of D_{1W} and D_{1E} of Figure 5.11 show that the magnitude of D_{1W} is slightly higher than that of D_{1E} which may lead one to incorrectly conclude that the positive flux gradient is now from east to west. However, the D_2 and the LVDT phase
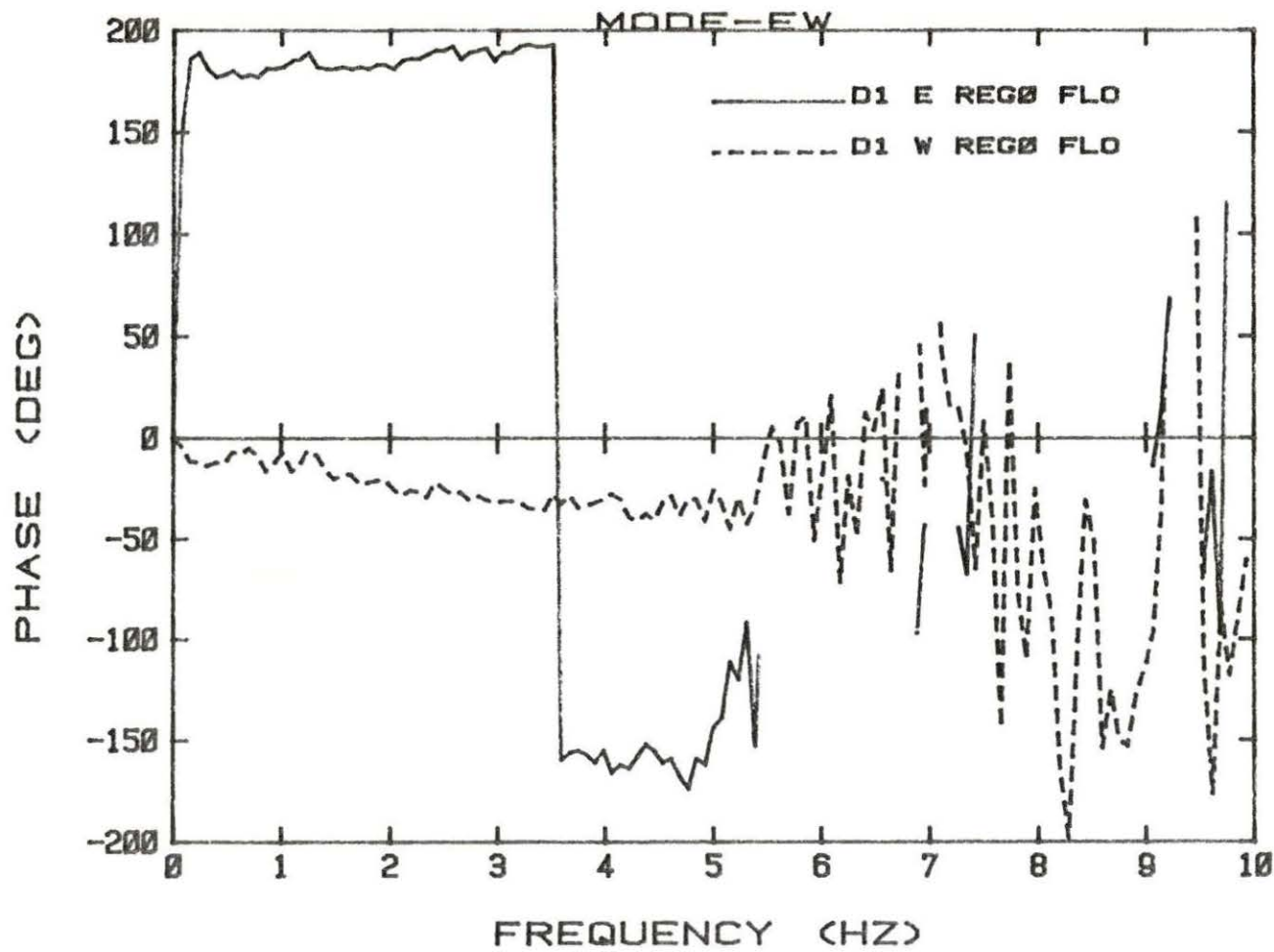
Figure 5.10. The transfer function phase between the LVDT and D_1 on the east and west side, for a PRBS input signal and the flooded case
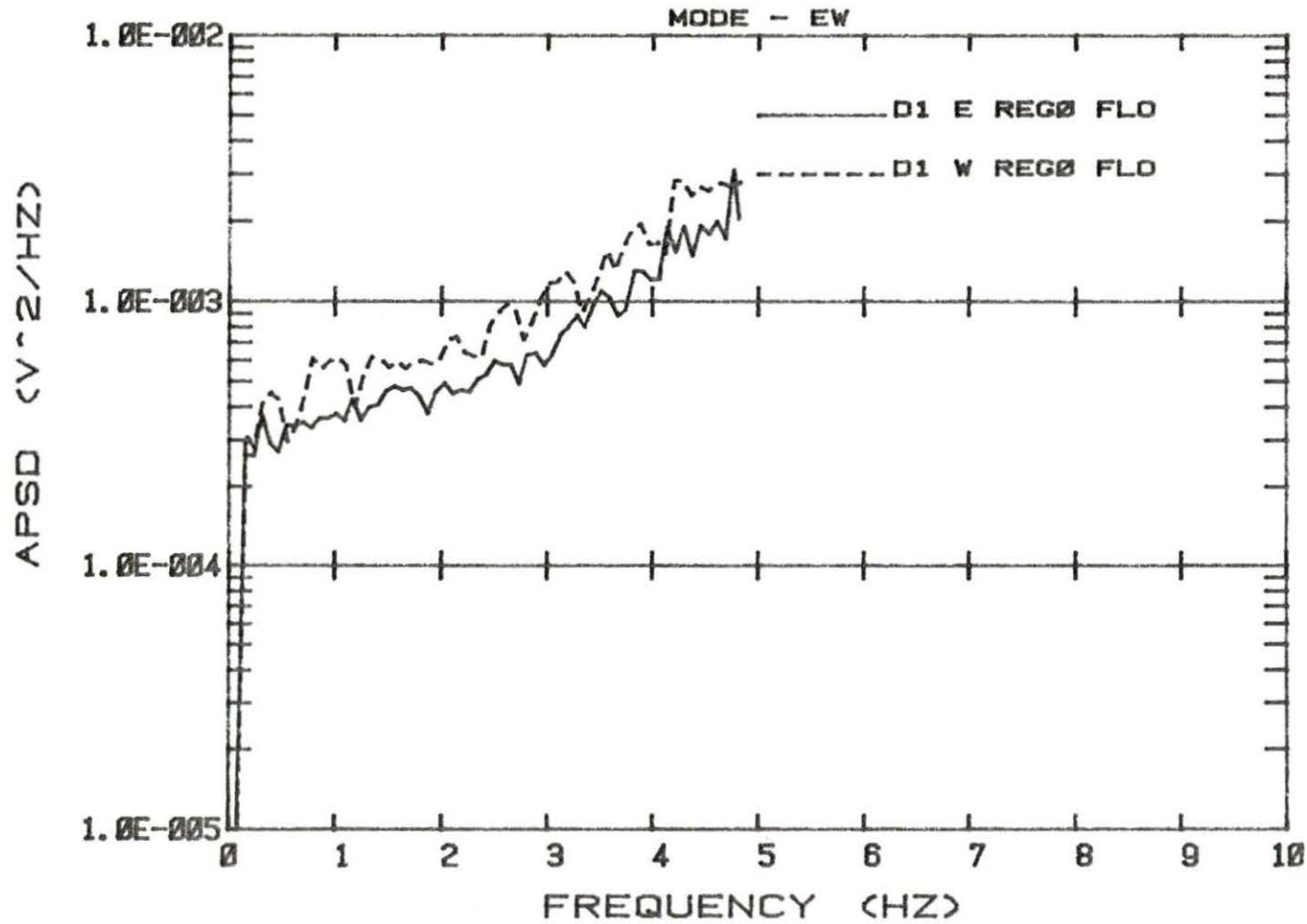
Figure 5.11. Normalized APSDs of D_1 on the east and west side for the PRBS input and the thimble flooded case

of 180° (Figure 5.12) shows that the flux gradient was still positive from west to east. The corresponding APSD plot for D_2 (not included) showed that the D_2 response was higher when the vibrator was on the east side, and this is possible only if the east side has a higher flux compared to the west side or the flux gradient is from west to east. The single frequency data also showed the same behavior. This anomaly could be due to the fact that L_W is much larger than the global components and also L_E. The local components in the two locations may have different magnitudes; however, they are assumed to be the same in the calculations. The difference must be more pronounced for the thimble-flooded case. The calculated L/G ratios are given in Table 5.1. The L/G ratios are much higher compared to the unflooded case. One possible explanation is that the flux gradient has decreased as a result of the flooding, resulting in a smaller global component. But it was found from the D_2 response that this was not the case. The only other possibility is that the local components have increased considerably in magnitude. The L/G ratios were higher when the regulating rod was at 100%. The large difference in the PRBS and the 1.5 Hz cases cannot be easily
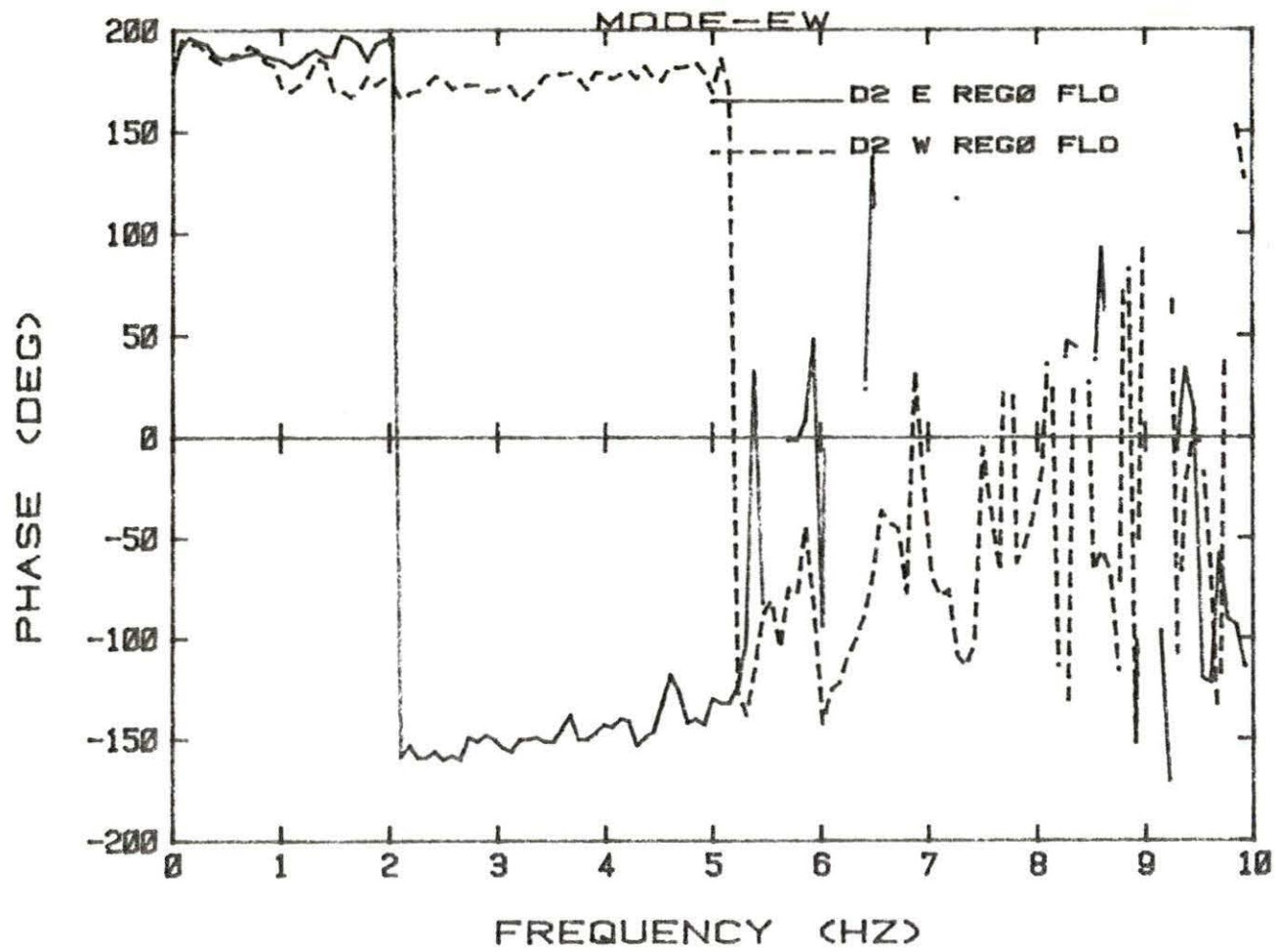
Figure 5.12. The transfer function phases between the LVDT and D_2, for a PRBS input signal

explained, but it is felt that the single frequency data
should be less subject to statistical errors and should
provide a better measure of the local to global ratio.
Due to the local-global interaction, the signals from the
detectors on either side of the absorber are opposite in
phase in the range the local effects are significant.
Therefore, the cross power spectral density (CPSD) phase
between the signals from the east and the west detector
should be 180°, if the detectors are located closer to the
absorber so that the local component is dominant. Note that
the CPSD phase is the same as the phase difference
between the D_{1E}/LVDT transfer function phase and the
D_{1W}/LVDT transfer function phase. For the case considered
in Figure 5.10, the CPSD phase is about 180°. But for the
unflooded case, considered in Figure 5.7, the CPSD phase
is not 180°. This can be explained as follows. From Figure
5.6, the CPSD phase is given by the phase difference
between D_{1W} and D_{1E}. If G_{1W} is larger than L_W the resultant,
X_{1W}, will be closer to G_{1W} than to L_W, in which case, as
is evident from Figure 5.6, the phase difference cannot
be 180°. This implies that for the case considered in
Figure 5.7 the local component was smaller in magnitude
than the global component.

The following conclusion can be made from Figure 5.6.

The local component drops off with distance from the absorber. This means that L in Figure 5.6 varies in magnitude with distance. As the magnitude of L changes, the direction of the resultant of L and G changes, which changes the CPSD phase angle between D_{1W} and D_{1E}. Therefore, the CPSD phase is a measure of the distance of the vibrating absorber from the detectors.

Figures 5.13 and 5.14 show the coherence between D_{1E} and the LVDT, and between D_{1W} and the LVDT, for the flooded and unflooded cases with the regulating rod at 0%. The lower coherence for the west side shows that this is the subtracting side. The coherence is much lower for the subtracting side (D_{1W}), for the unflooded case which implies a more severe subtraction on the west side. These plots support the conclusions, drawn from the APSD plots, that the local and global components subtract on the west side and add on the east side.

B. NS Vibrator Motion

In this case, the absorber motion was along the north-south (NS) direction. The detector was located on the line perpendicular to the direction of motion. To simulate the case of detectors located symmetrically on either side of the absorber, two configurations like that
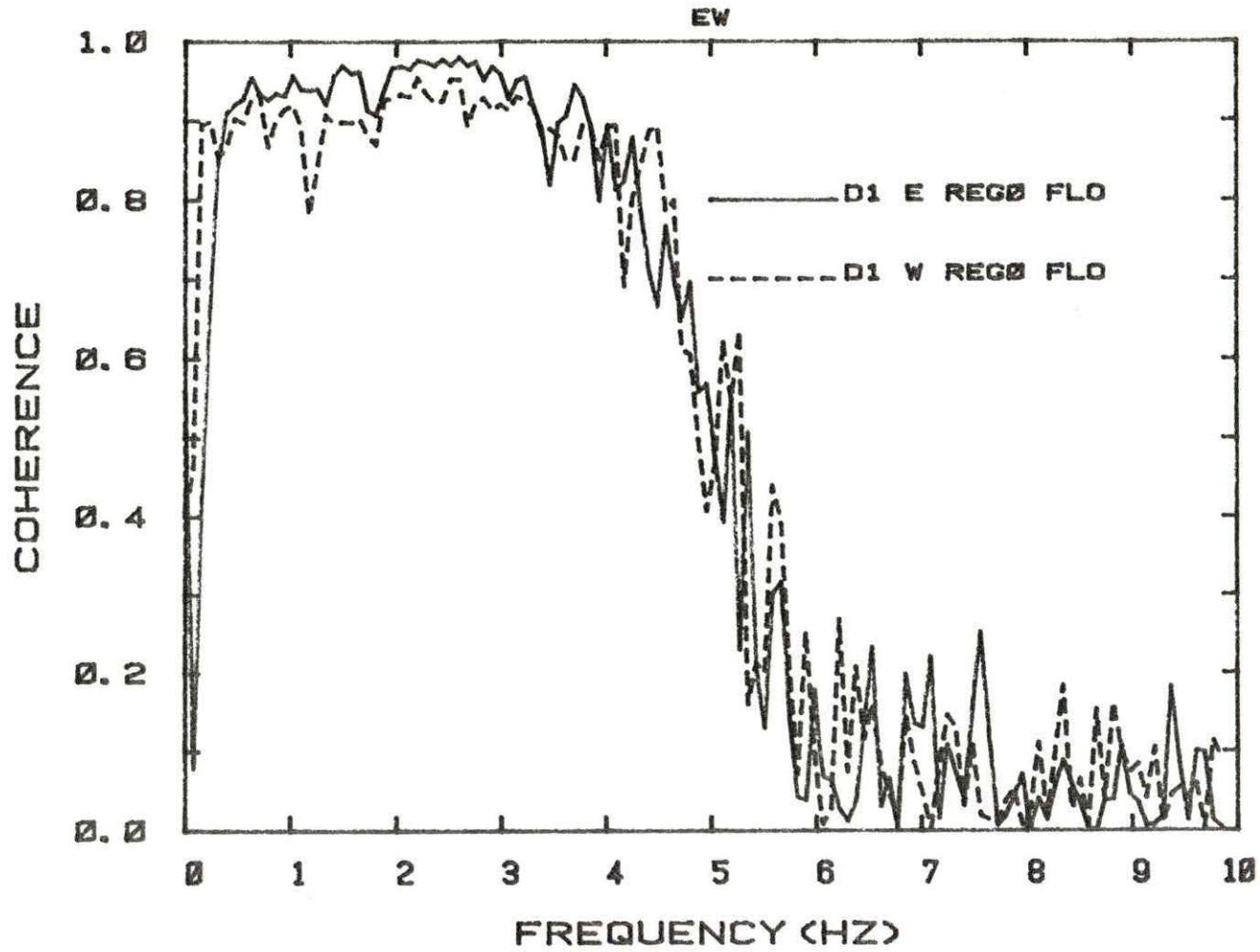
Figure 5.13. Coherence between LVDT and D_1 on the east and west side for the flooded case.
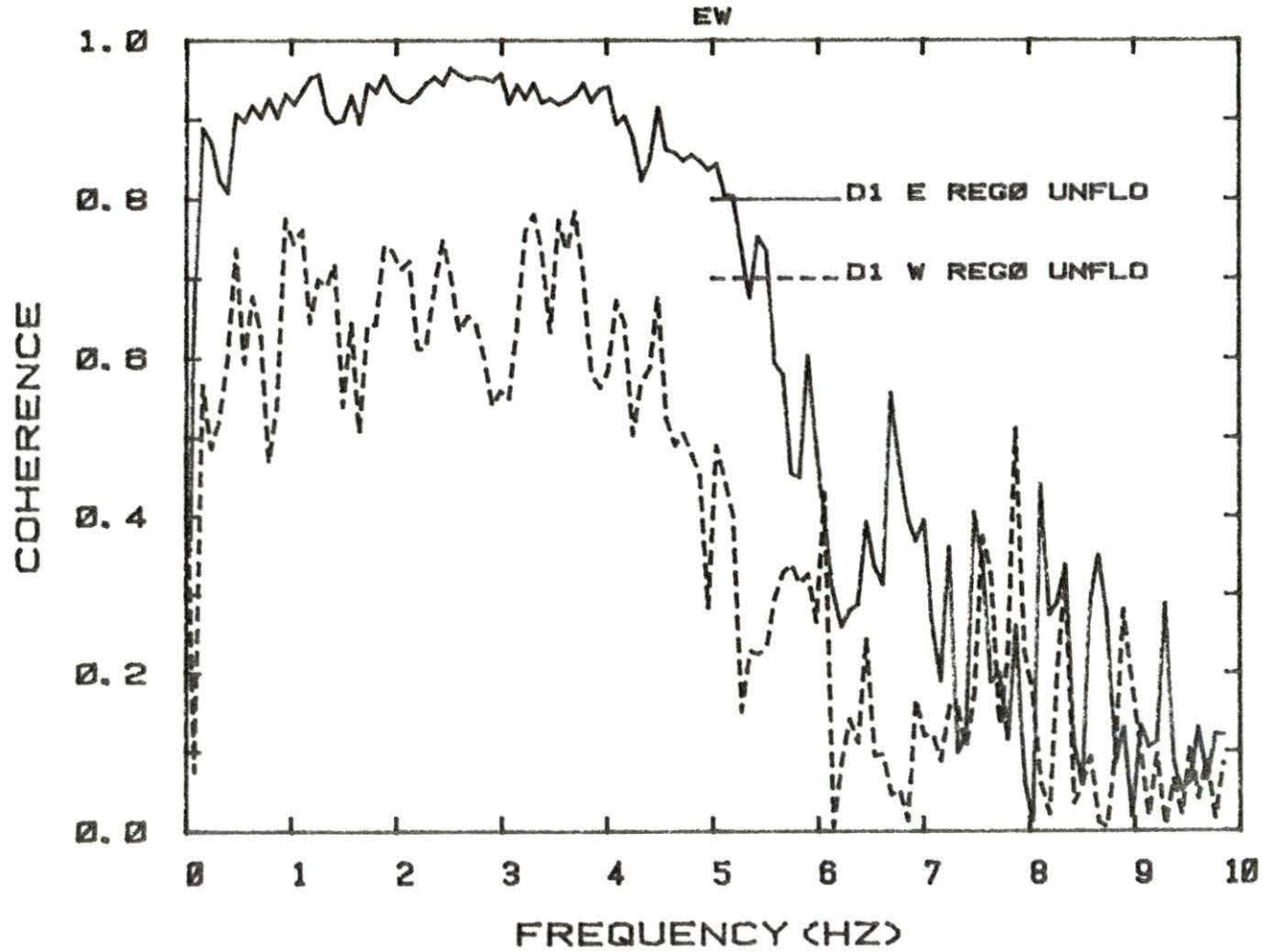
Figure 5.14. Coherence between the LVDT and D_1 on the east and west side for the unflooded case

shown in Figures 4.9a and 4.9b were used. Measurements were taken for all the different experimental modes shown in Figure 4.12. Figure 5.15 shows the normalized D_1 APSD for the case of a PRBS input with the regulating rod at 0% and the thimble unflooded. Again, the data above 4 Hz results mainly from the reactor background and may be discarded. The two curves are for D_1 on the west and east side of the absorber. They should be identical if the two detectors are symmetrically located. The curve 'D1 W' is obtained with the vibrator on the east side. This curve has a higher magnitude since the vibrator is located in a higher flux region and results in a higher negative reactivity insertion. Figure 5.16 shows the D_2 response, which sees only the global or the reactivity effect. This figure confirms the above conclusion that when the absorber is on the east side the reactivity insertion is higher. Thus, the observed difference in the plots is due to the fact that the vibrator and the detector locations are different for the east and west cases. The calculation of the local to global ratios were not feasible because of the large number of unknowns involved. The data for a 1.5 Hz input showed the same behavior.

The phase difference between D_{1E} and the LVDT and
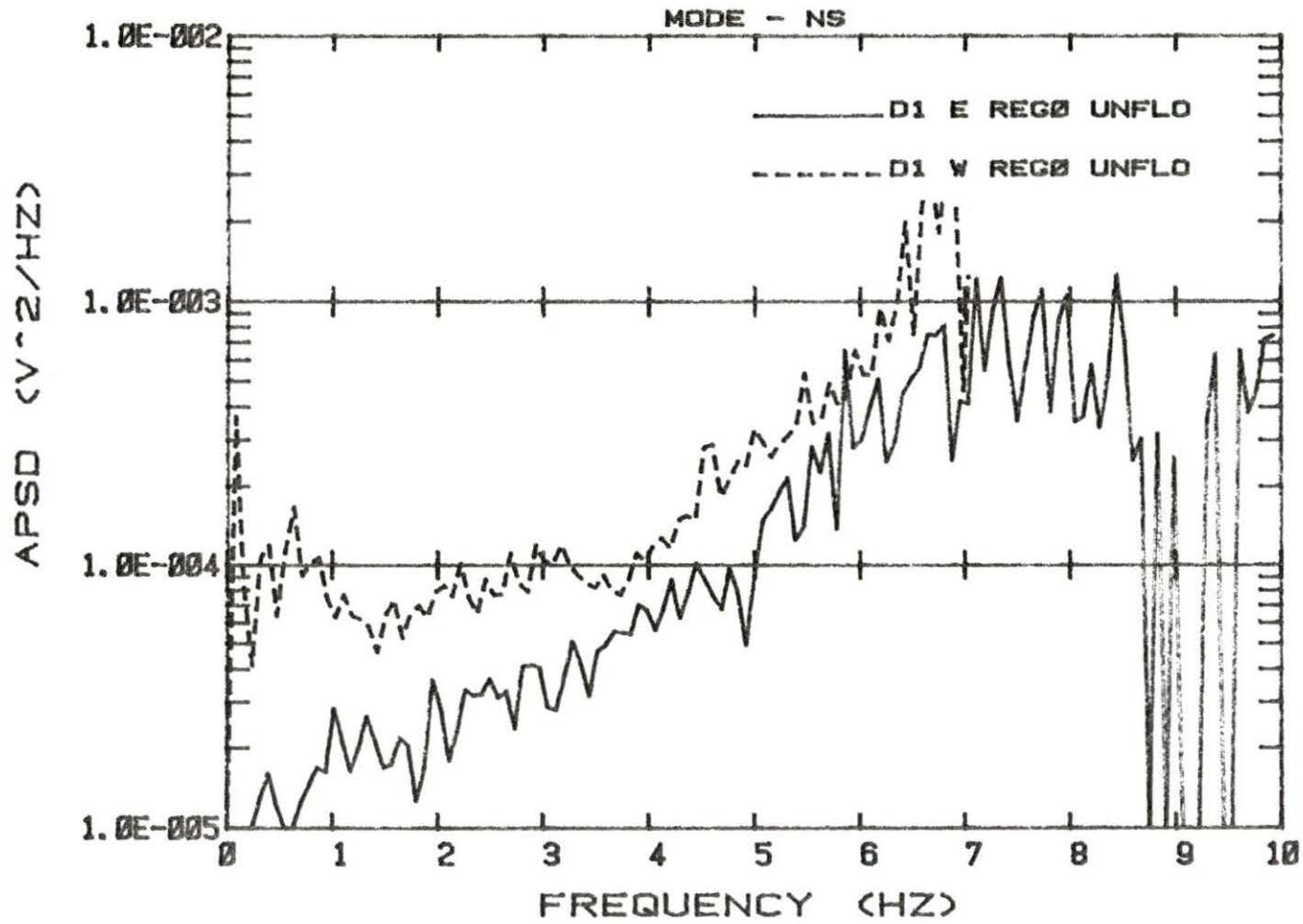
Figure 5.15. The APSDs of D_1 on the east and west side for the case of NS vibration
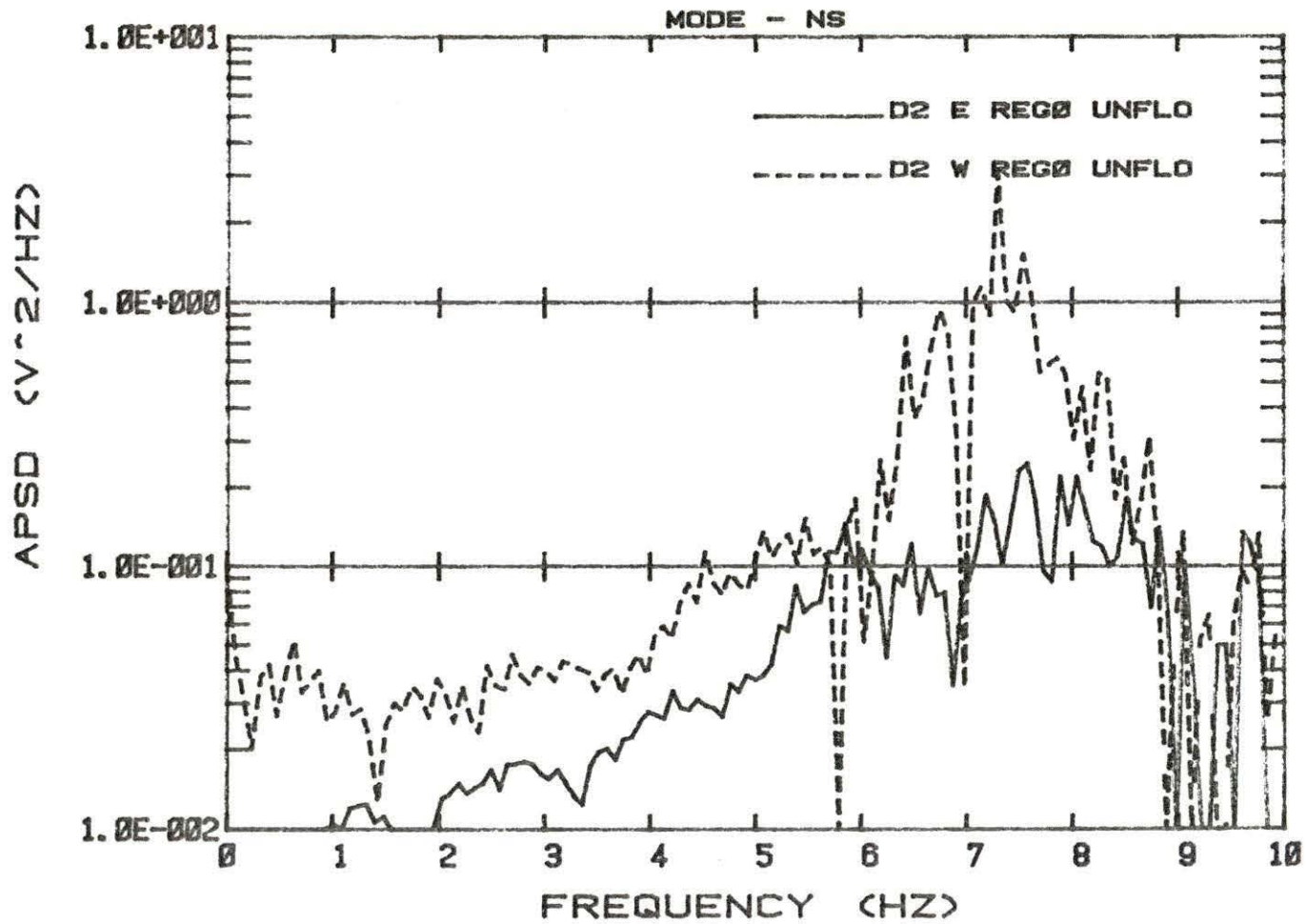
Figure 5.16. The APSDs of D_2 for the two locations of the absorber for the case of NS vibration

D_{1W} and the LVDT is shown in Figure 5.17. The CPSD phase is zero since, even though there could be both local and global effects, both detectors see the same effect of the local-global interaction. The signals between D_{1W} and the LVDT and D_{1E} and the LVDT are highly coherent (Figure 5.18) and show that both detectors see the same effect.

Figure 5.17. The transfer function phase between the LVDT and D_1 on the east and west side of the absorber moving in the NS direction
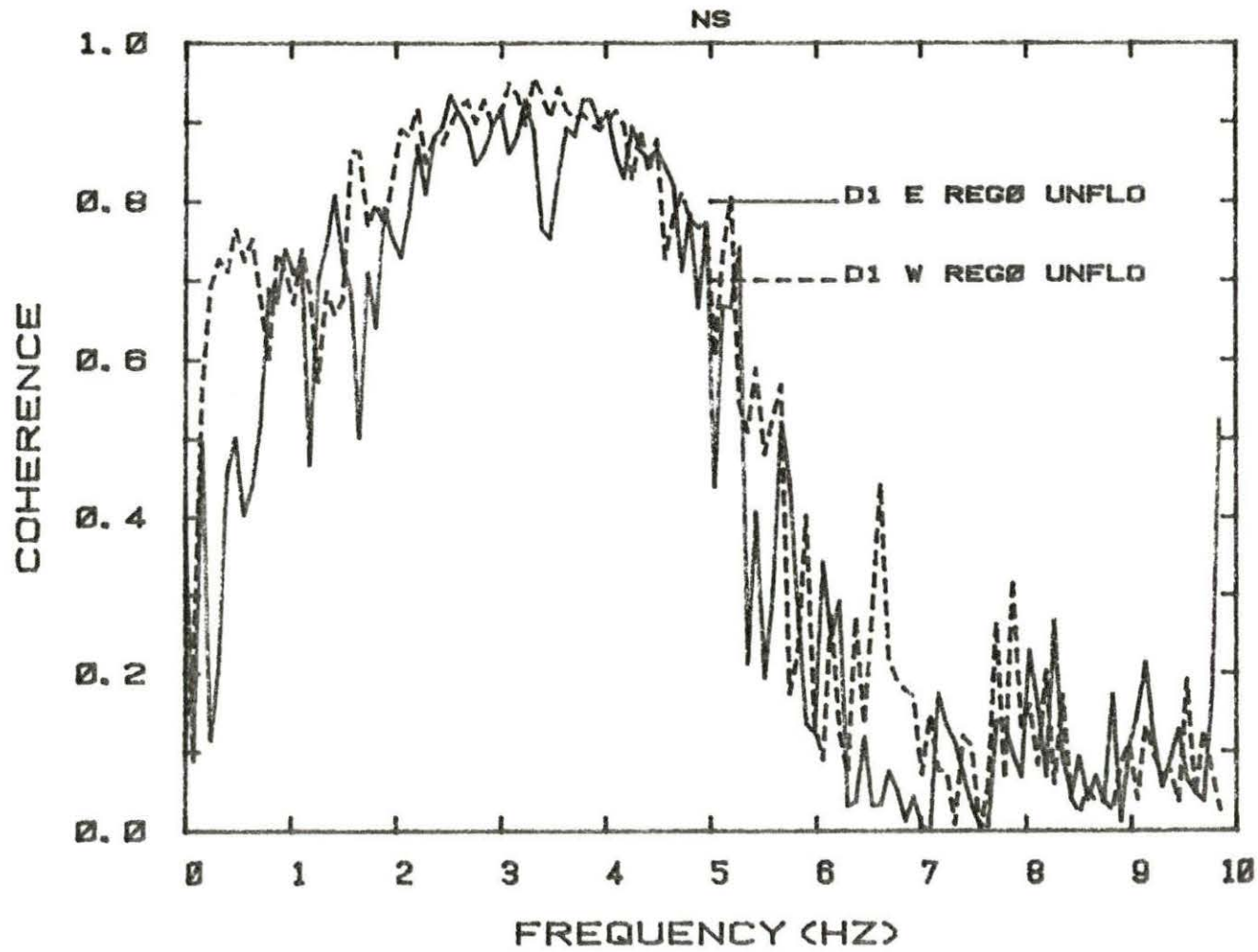
Figure 5.18. Coherence between the LVDT and D_1 on the east and west side for the case of NS vibration.

VI. CONCLUSIONS

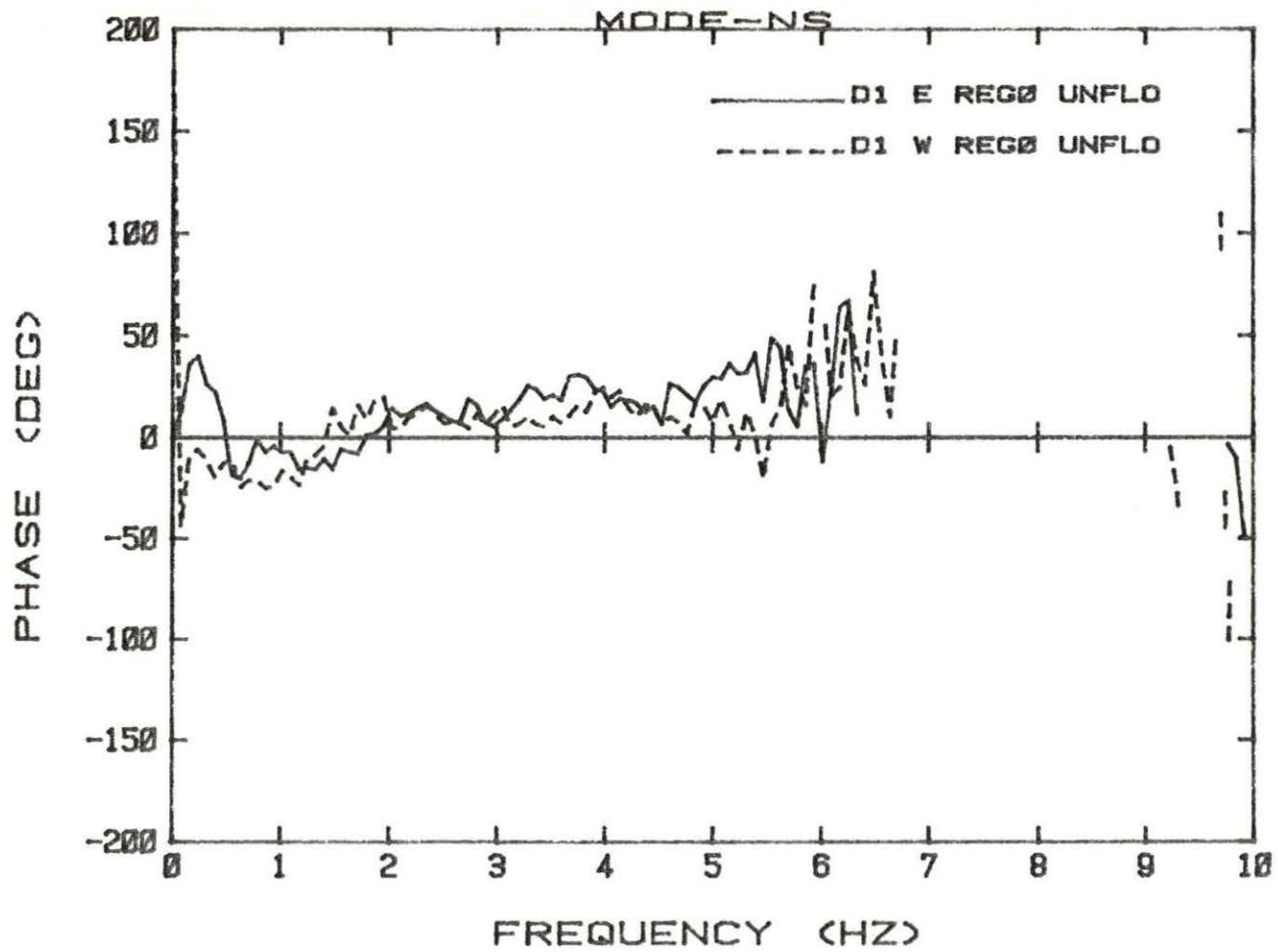The following conclusions can be drawn from the results of the experiment:

(1) Comparison of the results of this study with those of previous studies performed in the reflector region of the reactor shows that the components of the response have different enhancement characteristics in the fuel region. In the reflector region where the experiment was located, the flux gradient was very small resulting in a smaller value of the global component and hence a higher L/G ratio. In the fuel region, a higher flux gradient existed.

(2) The presence of the local and global components of the detector response and their interaction was evident from the results.

(3) The rapid space variation of the local component can be used for localization of a vibrating component, but the detector response is complicated by the local-global interaction. Procedures similar to the one used in this work could be utilized to separate the local and global components or to define a local to global ratio, which is a measure of the distance of the vibrating absorber from the detector.

(4) The CPSD phase is an indicator of the location of the vibrating component, and its use in localization is suggested.

(5) In the unflooded case, no significant effect was observed when the regulating rod position was changed. But, when the thimble was flooded there was some noticeable effect. The change in the flux gradient in the EW direction, due to regulating rod positions, is not very significant.

(6) The effect of flooding the thimble was considerable. A large increase in the L/G ratio can be explained only by assuming that there was a large increase in the local component on the subtracting side.

(7) Feasibility of operating a vibrating absorber in the fuel region and measuring its response has been demonstrated by this work.

The results support the conclusion that the detector response depends on its location as well as its relative orientation with respect to the absorber. Because of this, effect it is necessary to analyze the data from more than one detector, when monitoring vibrations in a reactor.

VII.   SUGGESTIONS FOR FUTURE WORK

The following include some suggestions for possible
improvements on the present work and further work to gain
a better understanding of the reactor noise generated by
vibrating components:

(1) Several assumptions were made during the analysis of
the experimental data. It was assumed that the local
component of the response and the constant relating D_1 and
D_2 remained the same for the two vibrator positions. A more
detailed theoretical analysis may be done to take into
account the change in these factors.

(2) A theoretical model of the UTR-10 for the experiment
could be developed and the experimental results compared
with the theoretical responses calculated.

(3) To avoid the problem of interchanging the vibrator and
the detector, small detectors may be used. The effect of
using small detectors on the signal strength may be
investigated. No measurements were taken for the case when
the vibration is north-south or east-west and the detectors
located on the north and south side of the absorber.
Reactivity requirements would necessitate the use of small
detectors. A smaller vibration apparatus that fits in
between the fuel plates without removing them would reduce
the reactivity loss of the reactor. The reduction in the

motion of the absorber can be compensated by increasing the length of the absorber.

(4) It would be interesting to study the response of a detector to multiple sources, both theoretically and experimentally. The response of a detector to absorbers located at various points in different regions in the reactor could be investigated experimentally to understand the propagation of noise from a source. The response and correlation between different detectors located at different points, to a single source may provide useful information since this is more representative of the actual situation.

(5) The response of detector(s) to a randomly vibrating absorber may be investigated.

(6) A specific power reactor with known vibrating components could be modelled theoretically to predict the response and experimental data could be analyzed to localize these components.

(7) Noise generated in the fast and thermal groups and the detector responses to these components may provide some new information to aid in localization.

(8) The design of a small critical assembly with easily alterable flux gradients and easily accessible locations may speed up the measurement phase of analyzing the problem.

VIII. REFERENCES

1. J. A. Thie, Neutron noise sources in PWR's, Progress
    in Nuclear Energy 1, 283 (1977).

2. J. A. Thie, Power Reactor Noise (American Nuclear
    Society, La Grange Park, Illinois, 1981).

3. M. Al-Ammar and R. A. Danofsky, Detection of component
    vibrations in reactors based on the local-global
    interaction, Transactions of the American
    Nuclear Society 39, 955 (1981).

4. M. Al-Ammar, Use of local-global ratio in detecting
    component vibration in reactors, Ph.D.
    dissertation, Iowa State University, 1981
    (unpublished).

5. R. J. Borland, Effects of neutron flux gradient and
    detector-vibrator geometry on the local-global
    responses of the UTR-10 reactor, M.S. thesis,
    Iowa State University, 1982 (unpublished).

6. R. A. Danofsky and R. A. Hendrickson, Response of the
    in-core Neutron Detectors of a Nuclear Reactor
    to Moving Core Components, Iowa State University
    Engineering Research Institute 83093, 1982.

7. I. Pazsit, G. Por and I. Lux, Reactor internals
    vibration monitoring by neutron noise methods
    in PWR's, Central Research Institute for Physics,
    H-1525 Budapest, Hungary, 1982.

8. M. Salih, Response of an in-core neutron detector to
    a vibrating absorber based on the detector adjoint
    function, M.S. thesis, Iowa State University,
    1981 (unpublished).

9. S. J. Lee and R. W. Albrecht, The use of neutronic
    fluctuations to locate a vibrating control rod
    in a PWR model, Nuclear Science and Engineering
    83, 427 (1983).

10. R. A. Danofsky, Department of Nuclear Engineering, Iowa State University, private communication, 1983.

11. I. Pazsit, Investigation of space-dependent noise induced by a vibrating absorber, Atomkernenenergie 30, No. 1, 29 (1977).

12. I. Pazsit, Two group theory of noise in reflected reactors with application to vibrating absorbers, Annals of Nuclear Energy 5, 185 (1978).

13. I. Pazsit and G. Th. Analytis, Theoretical investigation of the neutron noise diagnostics of two-dimensional control rod vibrations in a PWR, Annals of Nuclear Energy 7, 171 (1980).

14. G. Th. Analytis, A three-dimensional theoretical investigation of the local and global component of neutron noise in bare homogeneous water moderated reactors and applications, Annals of Nuclear Energy 7, 351 (1980).

15. S. E. Stephenson, D. P. Roux and D. N. Fry, Neutron fluctuation spectra in the Oak Ridge research reactor, Report ORNL-TM-1401 (1966).

16. J. C. Robinson, Analysis of neutron fluctuation spectra in the Oak Ridge research reactor and the High Flux Isotope Reactor, Report ORNL-4149 (1967).

17. A. Lucia, E. Ohlmer and D. Schwalm, Correlation between neutron noise and fuel element oscillation in the ECO-reactor, Atomkernenergie 22, 1 (1973).

18. J. B. Dragt and E. Turkcam, Borssele PWR noise: Measurement, analysis and interpretation, Progress in Nuclear Energy 1, 293 (1977).

19. V. Bauernfeind, Investigations of the vibrative excitation of PWR pressure and internals by pressure noise analysis and model calculations, Progress in Nuclear Energy 1, 323 (1977).

20. D. N. Fry, Experience in reactor malfunction diagnosis using on-line noise analysis, Nucl. Technol. 10, 273 (1971).

21. C. W. Mayo, Detailed neutron noise analysis of
    pressurized water reactor internal vibrations,
    Atomkernenergie 29, 9 (1977).

22. R. C. Gopal, Nuclear noise monitoring for core
    vibration surveillance, Trans. of American
    Nuclear Soc. 14, 210 (1971).

23. C. W. Mayo and R. L. Currie, Neutron noise monitoring
    of PWR internal vibrations, Progress in Nuclear
    Energy 1, 363 (1977).

24. H. Van Dam, Neutron noise in boiling water reactors,
    Atomkernenergie 27, No. 1, 8 (1976).

25. K. Behringer, G. Kosaly and Lj. Kostic, Theoretical
    investigation of the local and global components
    of the neutron noise field in a boiling water
    reactor, Nuclear Science and Engineering 63,
    306 (1977).

26. M. M. R. Williams, Random Processes in Nuclear Reactors
    (Pergamon Press, Oxford, 1974).

27. M. Antonopoulos-Domis, Reactivity and neutrn density
    noise excited by random rod vibration, Annals
    of Nuclear Energy 3, 451 (1976).

28. H. Van Dam, On the adjoint space in reactor noise
    theory, Annals of Nuclear Energy 4, 185 (1977).

29. W. Hennessy, Department of Nuclear Engineering, Iowa
    State University, private communication, 1983.

30. F. B. Hildebrand, Methods of Applied Mathematics
    (Prentice-Hall, Inc., Englewood Cliffs,
    N. J., 1965).

31. W. C. Nodean, The response of coupled core reactor to
    a localized oscillation of the absorption cross
    section, Ph.D dissertation, Iowa State
    University, 1969 (unpublished).

32. J. S. Bendat and A. G. Piersol, Random Data Analysis
    and Measurement Procedures (Wiley Interscience,
    New York, 1974).

33. R. A. Hendrickson, R. A. Danofsky, A. F. Rohach and
    D. M. Roberts, Safety Analysis Report for the
    Training Reactor UTR-10, Iowa State University
    Engineering Research Institute 82418, 1981.

34. J. T. Sankoorikal, Safety analysis report for an
    experiment using the UTR-10 reactor FR-82-01,
    Reactor Use Committee, Department of Nuclear
    Engineering, Iowa State University, 1982.

35. W. Hennessy, Procedure for testing and modifying an
    experimental fuel assembly for the UTR-10,
    Reactor Use Committee, Department of Nuclear
    Engineering, Iowa State University, 1982.

36. J. T. Sankoorikal, Interim and Final performance
    reports of the experiment FR-82-01,
    Reactor Use Committee, Department of Nuclear
    Engineering, Iowa State University, 1982.

37. H. W. Ott, Noise Reduction Techniques in Electronic
    Systems (Wiley Interscience, New York, 1976).

IX. ACKNOWLEDGEMENTS

X.   APPENDIX A: TECHNIQUES USED TO MINIMIZE THE PICKUP OF UNWANTED ELECTRONIC NOISE

The desired signal from the detectors, being low in amplitude, is often masked by electronic noise pickup due to electromagnetic interference. As pointed out in reference (37), to produce a noise problem there must be a noise source, a receiver susceptible to noise and a coupling channel that transmits the noise to the receiver.

The various noise sources present during the experiment were identified as the following: (1) the 60 Hz electromagnetic radiation originating from various electric and electronic devices in the surroundings, (2) the electromagnetic radiation in the frequency range of interest in the experiment, produced by a coil switching unit that was used originally and the coils themselves, (3) the DC component present in the detector signal and introduced by the various devices used for data collection. The receiver susceptible to the noise was mainly the D_1, and the preamplifier amplified the noise pickup. The noise coupling is through radiated electric and magnetic fields.

The following procedures helped to reduce the noise pickup considerably. The coil switching unit, mentioned

before, contained relays and contacts which produced
magnetic and electric fields. By replacing this unit by
a transistorized electronic switching unit, this problem
was eliminated. It was found out that the main source
of the problem was the collapsing magnetic field of the
coils. A small coil with lower driving voltage was used
in the design. Even though the metallic cover of the coils
were adequate to reduce the electric field radiated
from it, this had no effect on the magnetic fields
produced. The reverse emf produced by the collapsing
magnetic field of the coils could be about thousand times
the voltage used to drive the coils, over a small
duration. This voltage spike travelling through the
cables supplying power to the coils would produce electric
and magnetic fields that induce a noise voltage in the
signal cables. The frequency is the same as the
frequency with which the coils are energized, thereby
producing interference at the frequencies of interest.
The only solution was to reduce the reverse emf. This
was accomplished by connecting a diode across each coil,
as close to it as possible, such that the reverse emf
is shorted and thereby reduces the voltage spike.
The power carrying cables had shielding,and the ground
connection was through the shielding. This cuts down the

magnetic field radiation by cancelling the fields
produced by the inside cable and the shield. By grounding
the shield the electric field radiation can also be
reduced.

The detector was covered with an aluminum foil and
the twinax cables had copper braid shielding, and all the
instrumentation (preamp, batteries, etc.) were enclosed
in aluminum boxes. The shield and the aluminum boxes
were connected to a common ground. This eliminated the
electric pickup. Use of twisted pair twinax cables
provided much better shielding against magnetic fields,
since the induced voltages on either cable cancels out.

The filters and the analyzer were carefully
balanced to reduce the DC offset introduced by them.
The DC component in the detector signal was reduced by
using a fourth-order high-pass filter with a cut-off at
0.1 Hz. A low-pass filter with a cut-off at 16 Hz
eliminated the 60 Hz pickup. All these techniques
helped to minimize the unwanted noise pickup and made
it possible to increase the analyzer sensitivity. The
noise pickup with the vibrator running and without the
reactor operating was at least four orders of magnitude
less for D_1 and two orders of magnitude less for D_2.

XI. APPENDIX B: LISTING OF COMPUTER PROGRAMS

The following programs were developed, to be used on the HP-85 microcomputer, to aid in data manipulation and calculations. The programs not found in the listing given below may be found in reference (5).

a. DATSTR This program was used to store the data from the analyzer display on to a disk. See reference (5) for a listing of the program.

b. NOR2 This program calculates the normalized APSD from the raw data using equation 5.1 and stores this on disk for future use.

c. L/G L/G calculates the L/G ratio for the PRBS data using equations 3.17 through 3.20. The L/G values are printed out for each frequency point from 0.8 -4.0 Hz. For the 1.5 Hz case, the various data were read from the files and the L/G ratio was calculated using a short program (not included).

d. PLOT5 This program was used to plot the APSD data stored on disk. For a listing see reference (5).

e. PHASE This was used to plot the phase data stored on disk (see reference (5)).

f. COH1 Coherence data stored on disk was plotted using this program.

A. NOR2

```
10 DIM S(130),N(130),L(130),S1(130)
20 CLEAR @ BEEP
30 DISP "INPUT NOISE FILE"
40 INPUT N$
50 ASSIGN# 3 TO N$
60 FOR I=1 TO 128
70 READ# 3 ; N(I)
80 NEXT I
85 ASSIGN# 3 TO *
90 DISP "INPUT NAME OF DET SIG: FILE, LVDT FILE"
100 INPUT S$,L$
110 ASSIGN# 1 TO S$
120 ASSIGN# 2 TO L$
130 FOR I=1 TO 128
140 READ# 1 ; S(I)
150 READ# 2 ; L(I)
160 NEXT I
170 ASSIGN# 1 TO *
180 ASSIGN# 2 TO *
200 DISP "NAME OF NORMALIZED DATA STORAGE"
205 DISP "FILE --CHANGE DISK--"
210 INPUT D$
220 CREATE D$,1,1280
230 ASSIGN# 1 TO D$
240 FOR I=1 TO 128
250 S1(I)=(S(I)*S(I)-N(I)*N(I))/(L(I)*L(I))
260 PRINT# 1 ; S1(I)
270 NEXT I
280 ASSIGN# 1 TO *
290 BEEP
300 GOTO 90
310 DISP "END" @ END
```

B. L/G

```
10 ! L/GQNOR2 APSD QUAD LS
15 DEG
20 OPTION BASE 1
30 PRINTER IS 710,140
40 DIM A(64),B(64),C(64),D(64),E(64),W(64)
50 CLEAR @ BEEP
60 DISP "X1W,X1E,X2W,X2E,PE,PW"
70 INPUT A$,B$,C$,D$,E$,W$
80 ASSIGN# 1 TO A$
90 ASSIGN# 2 TO B$
100 ASSIGN# 3 TO C$
110 ASSIGN# 4 TO D$
120 ASSIGN# 5 TO E$
130 ASSIGN# 6 TO W$
140 FOR I=1 TO 64
145 DISP I
150 READ# 1 ; A(I)
160 IF A(I)<0 THEN 430
170 A(I)=SQR(A(I))
180 READ# 2 ; B(I)
190 IF B(I)<0 THEN 430
200 B(I)=SQR(B(I))
210 READ# 3 ; C(I)
220 IF C(I)<0 THEN 430
230 C(I)=SQR(C(I))
240 READ# 4 ; D(I)
250 IF D(I)<0 THEN 430
260 D(I)=SQR(D(I))
270 READ# 5 ; E(I)
280 READ# 6 ; W(I)
290 A1=D(I)^2-C(I)^2
300 B1=-(2*A(I)*D(I)^2*COS(W(I))+2*B(I)*C(I)^2*COS(E(I)))
310 C1=(D(I)*A(I))^2-(C(I)*B(I))^2
320 Z=B1^2-4*A1*C1
330 IF Z<0 THEN 430
340 Z=SQR(Z)
350 E1=(-B1+Z)/2/A1
360 G1=SQR(B(I)^2+E1^2+2*B(I)*E1*COS(E(I)))
```

```
370 G2=SQR(A(I)`2+E1`2-2*A(I)*E1*COS(W(I)))
380 E2=(-B1-Z)/2/A1
390 G3=SQR(B(I)`2+E2`2+2*B(I)*E2*COS(F(I)))
400 G4=SQR(A(I)`2+E2`2-2*A(I)*E2*COS(W(I)))
410 PRINT USING 420 ; I;E1;E1/G1;E1/G2;E2;E2/G3;E2/G4
420 IMAGE 2D,3X,6(D.DE,3X)
430 NEXT I
440 ASSIGN# 1 TO *
450 ASSIGN# 2 TO *
460 ASSIGN# 3 TO *
470 ASSIGN# 4 TO *
480 ASSIGN# 5 TO *
490 ASSIGN# 6 TO *
500 END
```

C. COH1

```
10 OPTION BASE 0
20 DIM B(130),H$[50]
30 DISP "INPUT NAME OF DATA FILE FROM WHICH"
35 DISP "DATA IS TO BE PLOTTED"
40 INPUT A$
44 DISP "INPUT LINETYPE"
45 INPUT K
50 ASSIGN# 1 TO A$
60 N=127
70 FOR I=0 TO N
80 READ# 1 ; B(I)
90 NEXT I
100 F=10
110 ASSIGN# 1 TO *
120 PLOTTER IS 705
130 LOCATE 35,115,30,90
140 SCALE 0,F,0,1
150 L$="COHERENCE"
160 XAXIS 0,1,0,10
170 FOR I=0 TO 10
180 MOVE I,-.04 @ LORG 6
190 LABEL USING "2D" ; I
200 NEXT I
210 YAXIS 10,-.1,0,1
220 MOVE F/2,-.13
230 LORG 5 @ CSIZE 3,1,0
240 LABEL "FREQUENCY(HZ)"
250 YAXIS 0,.1,0,1
260 FOR I=0 TO 10 STEP 2
270 Y8=.1*I
280 MOVE -.4,Y8 @ LORG 8
290 CSIZE 2.7,.9,0
300 LABEL USING "Z.D" ; Y8
310 NEXT I
320 XAXIS 1,-1,0,10
330 DEG @ LDIR 90
340 CSIZE 3,1,0
350 MOVE -1.5,.5 @ LORG 5
360 LABEL L$
370 MOVE 0,B(0)
```

```
370 MOVE 0,B(0)
375 LINETYPE K,1
380 FOR I=1 TO N-2
390 PLOT I*F/N,B(I),-1
400 NEXT I
410 PENUP @ CLEAR @ BEEP
420 LDIR 0
430 DISP "WOULD YOU LIKE A LEGEND FOR THE PLOT? (Y OR N)"
440 INPUT C$
450 IF C$<>"Y" THEN 640
460 DISP "POSITION 1 OR 2"
470 INPUT T
480 LORG 1 @ CSIZE 2,1,0
490 DISP "INPUT LEGEND LABEL"
500 INPUT T$
510 IF T=2 THEN 580
520 MOVE F/2,.8
530 LINETYPE K,1
540 DRAW .62*F,.8
550 MOVE .63*F,.8
560 LABEL T$
570 GOTO 640
580 MOVE .5*F,.7
590 LINETYPE K,1
600 DRAW .62*F,.7
610 MOVE .63*F,.7
620 LABEL T$
630 PENUP @ BEEP
640 DISP "DO YOU WANT A TITLE"
650 INPUT Z$
660 IF Z$<>"Y" THEN 740
670 DISP "INPUT TITLE"
680 INPUT H$
710 MOVE F/2,1.03
720 LORG 5 @ CSIZE 2,1,0
730 LABEL H$
731 DISP "ANOTHER PLOT"
732 INPUT Q
733 IF Q=1 THEN 30
735 DISP "END"
740 END
```